ORIGINAL ARTICLE

Loss of Pdk1-Foxo1 Signaling in Myeloid Cells Predisposes to Adipose Tissue Inflammation and Insulin Resistance

Yoshinaga Kawano,[1] Jun Nakae,[1] Nobuyuki Watanabe,[2] Shiho Fujisaka,[3] Kristy Iskandar,[4] Risa Sekioka,[1] Yoshitake Hayashi,[5] Kazuyuki Tobe,[3] Masato Kasuga,[6] Tetsuo Noda,[7] Akihiko Yoshimura,[8] Masafumi Onodera,[2] and Hiroshi Itoh[1]

Chronic inflammation in adipose tissue contributes to obesity-related insulin resistance. The 3-phosphoinositide-dependent protein kinase 1 (Pdk1)/forkhead transcription factor (Foxo1) pathway is important in regulating glucose and energy homeostasis, but little is known about this pathway in adipose tissue macrophages (ATMs). To investigate this, we generated transgenic mice that carried macrophage/granulocyte-specific mutations, including a *Pdk1* knockout (*LysMPdk1*$^{-/-}$), a *Pdk1* knockout with transactivation-defective Foxo1 (*Δ256LysMPdk1*$^{-/-}$), a constitutively active nuclear (CN) Foxo1 (*CNFoxo1*^{LysM}), or a transactivation-defective Foxo1 (*Δ256Foxo1*^{LysM}). We analyzed glucose metabolism and gene expression in ATM populations isolated with fluorescence-activated cell sorting. The *LysMPdk1*$^{-/-}$ mice exhibited elevated M1 macrophages in adipose tissue and insulin resistance. Overexpression of transactivation-defective Foxo1 rescued these phenotypes. *CNFoxo1*^{LysM} promoted transcription of the C-C motif chemokine receptor 2 (*Ccr2*) in ATMs and increased M1 macrophages in adipose tissue. On a high-fat diet, *CNFoxo1*^{LysM} mice exhibited insulin resistance. *Pdk1* deletion or Foxo1 activation in bone marrow–derived macrophages abolished insulin and interleukin-4 induction of genes involved in alternative macrophage activation. Thus, Pdk1 regulated macrophage infiltration by inhibiting Foxo1-induced *Ccr2* expression. This shows that the macrophage Pdk1/Foxo1 pathway is important in regulating insulin sensitivity in vivo. ***Diabetes* 61:1935–1948, 2012**

Obesity is a predisposing factor for the development of type 2 diabetes, hypertension, hyperlipidemia, and atherosclerosis (1). Chronic activation of intracellular proinflammatory pathways in adipose tissue contributes to obesity-related insulin resistance. Adipose tissue macrophages (ATMs) are a major source of proinflammatory cytokines, including interleukin (IL)-6, IL-1β, and tumor necrosis factor (TNF)-α, which can decrease insulin sensitivity in insulin target cells (2). However, only sparse evidence suggests that ATMs may become insulin resistant and play a role in insulin signaling (3–9).

The 3-phosphoinositide-dependent protein kinase 1 (Pdk1)–forkhead transcription factor (Foxo1) signaling pathway regulates energy and glucose metabolism in several insulin-responsive tissues, including pancreatic β-cells and proopiomelanocortin and agouti-related protein neurons (10,11). However, few studies investigate this signaling pathway in ATMs. Recent reports suggest that activation of Foxo1 in macrophages promotes inflammation by inducing IL-1β expression (12) or toll-like receptor 4–mediated signaling (13). They show that Foxo1 could induce inflammatory cascades, but they do not investigate the role of Foxo1 specifically in ATMs in vivo.

In the current study, we generated transgenic mice that carried macrophage-specific mutations, including a *Pdk1* knockout, a constitutively nuclear (CN) *Foxo1*, or a transactivation-defective *Foxo1*. We analyzed insulin sensitivity in these mice in vivo. We found a novel Pdk1-Foxo1 signaling mechanism that regulated M1 macrophage recruitment.

RESEARCH DESIGN AND METHODS

Mice. All experimental protocols with mice were approved by the animal ethics committees of the Keio University School of Medicine (09134-1). To create macrophage-specific *Pdk1* knockout mice, *Pdk1*$^{flox/flox}$ mice (11) were crossed with *LysMCre* transgenic mice (14). The generation of *R26*^{floxneoCNFoxo1} mice was described previously (11). Only animals from the same generation of the mixed-background strain were compared. All mice studied were examined on a B6/129 mixed genetic background. Mice were obtained from two independent cohorts of independent breeders, and littermates were used for every in vivo study. Animals were housed in sterile cages in a barrier animal facility at 22–24°C with a 12-h light/dark cycle.

Antibodies. All antibodies used in the current study are available upon request.

Analytical procedures. For high-fat diet (HFD) studies, we used age-matched (28-week-old) mice. We started the HFD at age 4 weeks for the 24-week HFD and at age 24 weeks for the 4-week HFD. All of the HFD mice were compared with age-matched mice fed a normal chow diet (NCD). The HFD was described previously (15). Analysis was limited to male mice because they are more susceptible to insulin resistance and diabetes. We performed intraperitoneal glucose tolerance tests (IPGTTs) after an overnight fast and insulin tolerance tests (ITTs) after fasting for 3–5 h. The area under the curve (AUC) was calculated from the level of each measured point by the trapezoidal method.

Flow cytometric analysis. Flow cytometric analysis was performed as described previously (16).

Hepatic glycogen content. We measured glycogen content as described previously (17).

Immunofluorescence. Double-positive cells were counted and marked digitally to prevent multiple counts with Adobe Photoshop CS4 EXTENDED and ImageJ software (National Institutes of Health, Bethesda, MD). Cells were counted in eight mice for each HFD duration. At least 300 cells were counted in each mouse.

From [1]Frontier Medicine on Metabolic Syndrome, Division of Endocrinology, Metabolism, and Nephrology, Department of Internal Medicine, Keio University School of Medicine, Tokyo, Japan; the [2]Department of Human Genetics, National Center for Child Health and Development, Tokyo, Japan; the [3]Department of Internal Medicine, University of Toyama, Toyama, Japan; the [4]Pediatric Research Office, Department of Child Health, Faculty of Medicine, Universitas Gadjah Mada, Sardjito Hospital, Yogyakarta, Indonesia; the [5]Division of Molecular Medicine and Medical Genetics, International Center for Medical Research and Treatment, Kobe University Graduate School of Medicine, Kobe, Japan; the [6]Research Institute, International Medical Center of Japan, Tokyo, Japan; the [7]Department of Cell Biology, Japanese Foundation for Cancer Research, Cancer Institute, Tokyo, Japan; and the [8]Department of Microbiology and Immunology, Keio University School of Medicine, Tokyo, Japan.

Corresponding author: Jun Nakae, jnakae35@sc.itc.keio.ac.jp.

Received 6 June 2011 and accepted 6 March 2012.

DOI: 10.2337/db11-0770

This article contains Supplementary Data online at http://diabetes.diabetesjournals.org/lookup/suppl/doi:10.2337/db11-0770/-/DC1.

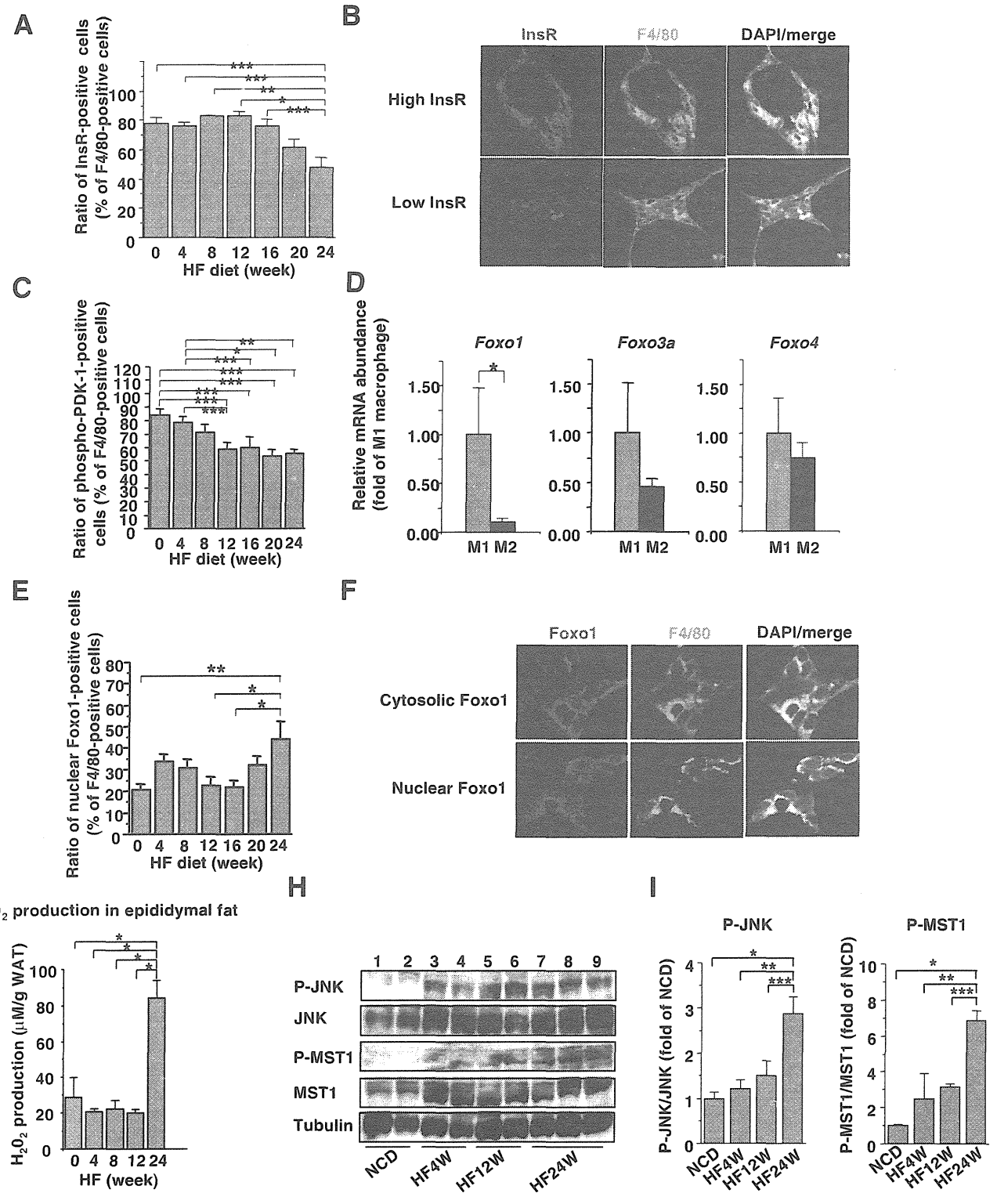

FIG. 1. Characterization of InsR, Pdk1, and Foxo1 in ATMs during an HFD. *A*: The percentages of InsR$^+$ cells among F4/80$^+$ cells in epididymal fat from age-matched wild-type mice fed an NCD and 24 weeks of an HFD. Values are means + SEM of eight mice. *$P < 0.005$, **$P < 0.01$, and ***$P < 0.05$ (one-factor ANOVA). *B*: Representative immunofluorescence images of epididymal fat double labeled for InsR and F4/80 in wild-type mice fed an HFD for 24 weeks. Cells that exhibit high expression level of InsR protein (*top*); cells that exhibit low or faint expression level of InsR (*bottom*). Red, green, and blue indicate InsR, F4/80, and DAPI staining, respectively. *C*: The percentages of phospho-PDK1$^+$ cells among F4/80$^+$ cells in epididymal fat from age-matched wild-type mice fed an NCD and 24 weeks of an HFD. Values are means + SEM of eight mice. *$P < 0.005$, **$P < 0.01$, ***$P < 0.05$ (one-factor ANOVA). *D*: Real-time PCR analysis of *Foxo* family members in cell populations sorted by flow cytometric analysis of the SVF from the epididymal fats of wild-type mice fed an HFD for 16 weeks, using anti-F4/80, anti-CD11c, and anti-CD206 antibodies. The levels of each transcript were normalized to the level in M1 macrophages. Values are means + SEM of three mice. *$P < 0.05$ (one-factor ANOVA, M1 vs. M2 macrophages). *E*: The percentages of nuclear Foxo1$^+$ cells among F4/80$^+$ cells in the epididymal fat of age-matched wild-type

H_2O_2 production. Measurement of H_2O_2 production was performed as described elsewhere (18). Epididymal fat was dissected from age-matched male C57BL/6J mice on either an NCD or a 4-24 week HFD.

Counting crown-like structures. Measurement of number of crown-like structures (CLSs) was performed as described previously (16).

Cell size measurements. Adipocyte size was measured with FLVFS-LS software (Flovel, Tokyo, Japan) by manually tracing a minimum of 1,200 adipocytes for each mouse. We measured adipocytes in at least six mice of each genotype.

Isolation of murine bone marrow–derived macrophages. Isolation of bone marrow–derived macrophages (BMDMs) was performed as described elsewhere (19).

Transwell migration assay. Transwell migration assays were performed as previously described (20).

Viral transduction. Adenovirus constructs that encoded Foxo1 mutants are described elsewhere (21,22). RAW264.7 cells were infected with adenoviruses (10–100 multiplicity of infection [MOI]) and harvested after 48 h. For cotransductions, cells were first transduced with an adenovirus that encoded Flag-CNFoxo1 at the indicated MOI for 8 h. The virus was then removed from the culture dish, and the cells were transduced with another adenovirus that encoded HA-Δ256Foxo1 at the indicated MOI for 8 h.

RNA isolation and real-time PCR. The isolation of total RNA and real-time PCR were performed as described previously (15). All primer sequences are available upon request.

Western blotting. Western blotting was performed as described previously (15). Insulin-stimulated phosphorylation of insulin receptor substrates (IRSs) and Akt were performed as described elsewhere (23).

Construction of C-C motif chemokine receptor 2 promoter–directed luciferase reporter vectors. Several DNA fragments containing the mouse C-C motif chemokine receptor 2 (*Ccr2*) promoter were PCR-amplified from mouse genomic DNA. After verifying their nucleotide sequences by DNA sequencing, the *Ccr2* promoter fragments were cloned into the luciferase reporter pGL3-Basic vector (Promega, Madison, WI). All primer sequences are available upon request.

Site-directed mutagenesis. The QuickChange II site-directed mutagenesis kit (Stratagene, La Jolla, CA) was used to alter the consensus Foxo1 binding elements in the *Ccr2* promoter in PGL3-Basic vectors. Mutated nucleotides were confirmed with DNA sequencing. All primer sequences are available upon request.

Luciferase assay. The luciferase assay was performed as described previously (22).

Electrophoretic mobility shift assay. Electrophoretic mobility shift assay (EMSA) and the super shift assay were performed as described previously (24).

Chromatin immunoprecipitation assay. Chromatin immunoprecipitation (ChIP) assay was performed as described previously (22).

Statistical analysis. We calculated descriptive statistics with ANOVA followed by Fisher test (Statview; SAS Institute Inc.). $P < 0.05$ was considered significant. Differences between two groups or among three groups were investigated with two-way repeated-measures ANOVA with an ad hoc multiple comparison method (Fisher least significant differences [LSD] test).

RESULTS

Insulin receptor expression and Pdk1 phosphorylation in ATMs during an HFD. To explore the significance of insulin signaling pathway in ATM, we examined insulin receptor (InsR) protein expression in ATMs by double immunofluorescence with anti-InsR and anti-F4/80 antibodies. During the HFD, ATM InsR protein levels were significantly reduced by ~50% compared with controls (Fig. 1*A* and *B*).

Next, we explored Pdk1 expression in ATMs under different diets. Immunofluorescence of epididymal fat from C57BL/6J mice on an HFD for 16 weeks revealed that cells positive for the macrophage marker CD68 were also positive for Pdk1 (Fig. 2*A*, *top*). Because Pdk1 activity depends on Ser 241 phosphorylation (25), we probed with an antiphospho-Pdk1 antibody. On an NCD, ~80% of F4/80$^+$ cells were stained with antiphospho-Pdk1. On an HFD for 24 weeks, the proportion of phospho-Pdk1$^+$ ATMs gradually decreased from 80% to from 40 to 50% (Fig. 1*C*). These data confirm that the InsR-Pdk1 pathway was functionally regulated in ATMs during the HFD.

Foxo1 in ATMs under an HFD. To explore the relative importance of Foxo family members in ATMs, we compared the expression of *Foxo1*, *Foxo3a*, and *Foxo4* in M1 and M2 macrophages isolated from the stromal vascular fraction (SVF) of epididymal fat from C57BL/6J mice fed an HFD for 16 weeks. We defined F4/80$^+$CD11c$^+$CD206$^-$ cells as M1 macrophages and F4/80$^+$CD11c$^-$CD206$^+$ cells as M2 macrophages (16). M1 macrophages showed significantly increased *Foxo1* expression compared with M2 macrophages. *Foxo3a* expression was also increased in M1 compared with M2 macrophages but not significantly. In contrast, M1 and M2 macrophages showed similar *Foxo4* expression (Fig. 1*D*). These observations suggest that Foxo1 played an essential role in ATMs.

Because Foxo1 activity depends on its subcellular localization (26), we examined Foxo1 with immunofluorescence in ATMs from age-matched C57BL/6J mice fed an NCD or HFD. Under the NCD, ~20% of Foxo1 was localized to the nucleus. After 24 weeks of an HFD, ~45% of Foxo1 was localized to the nucleus (Fig. 1*E* and *F*). These data suggest that Foxo1 was functionally significant in ATMs.

Foxo1 is regulated by oxidative stress through H_2O_2 production and the Jun NH_2-terminal kinase (JNK)–mammalian Ste20-like kinase 1 (MST1) pathway, which induces Foxo1 nuclear translocation (27–30). The production of H_2O_2 significantly increased at ~24 weeks of HFD (Fig. 1*G*). Furthermore, JNK and MST1 phosphorylation significantly increased after 24 weeks of HFD (Fig. 1*H* and *I*). These data suggest that both decreased Pdk1 phosphorylation and activation of the JNK-MST1 pathway may contribute to Foxo1 nuclear localization.

Deletion of Pdk1 in ATMs causes insulin resistance with rescue by transactivation-defective Foxo1. To clarify the function of Pdk1 in ATMs, we generated mice that lacked *Pdk1* in macrophages/granulocytes (*LysMPdk1*$^{-/-}$). Efficient, specific *Pdk1* deletion was evidenced by immunofluorescence (Fig. 2*A*) and Western blot analysis (Fig. 2*B*). Thus, we could study the effects of cell-specific *Pdk1* deficiency.

The deletion of *Pdk1* in ATMs was expected to cause nuclear localization of Foxo1. Immunofluorescence with an anti-Foxo1 antibody in epididymal fat revealed that ~60–70% of Foxo1 was localized to the nuclei of ATMs in *LysMPdk1*$^{-/-}$ mice (Fig. 2*C*). We assumed that Foxo1 was active in *Pdk1*-deficient ATMs and that this activity could be blocked with the dominant-negative form of Foxo1 (Δ256Foxo1), which lacked a COOH-terminal transactivation domain (31). To investigate this, we crossed

mice fed an NCD and 24 weeks of an HFD. Values are means + SEM of eight mice. *$P < 0.001$, **$P < 0.005$ (one-factor ANOVA). *F*: Representative immunofluorescence images of epididymal fat double labeled for Foxo1 and F4/80 in wild-type mice fed an HFD for 24 weeks. Cytosolic (*top*) and nuclear Foxo1 (*bottom*). Red, green, and blue indicate Foxo1, F4/80, and DAPI staining, respectively. *G*: The release of H_2O_2 from epididymal fats from age-matched male C57BL/6J mice fed an NCD or 4–24 weeks of an HFD. Values are expressed as mean ± SEM of five mice in each condition. *$P < 0.001$ (one-factor ANOVA). *H*: Western blotting of epididymal fats from age-matched male C57BL/6J mice fed an NCD or 4–24 weeks of an HFD. After transference to nylon membrane, tissue lysates (200 μg) were blotted to the indicated antibodies. *I*: Quantitative analysis of JNK and MST1 phosphorylation in epididymal fats. The intensity of each band was measured using NIH Image 1.62, and the intensities of bands of phospho-JNK or phospho-MST1 bands were corrected by total JNK or MST1 and calculated as the fold change from NCD. Data are means + SEM of five mice in each genotype. *$P < 0.001$, **$P < 0.005$, and ***$P < 0.05$ (one-factor ANOVA of NCD vs. HFD). WAT, white adipose tissue; P, phospho; W, weeks. (A high-quality digital representation of this figure is available in the online issue.)

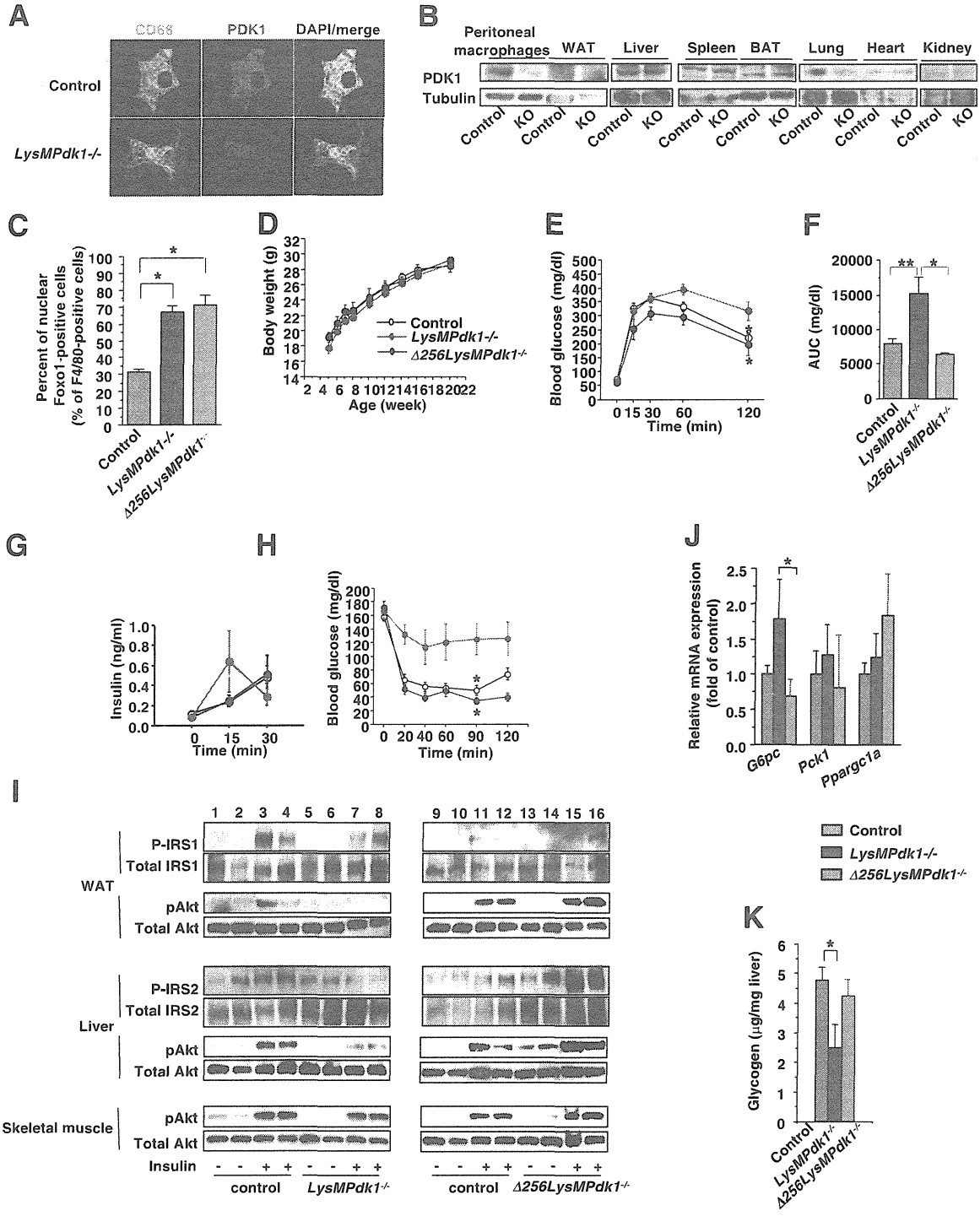

FIG. 2. Effects of the deletion of *Pdk1* or inhibition of the transactivation of Foxo1 on glucose metabolism and insulin sensitivity. *A*: Representative immunofluorescence images of epididymal fat double labeled for CD68 and PDK1 in 24-week-old wild-type and *LysMPdk1*$^{-/-}$ mice. Green, red, and blue indicate CD68, PDK1, and DAPI staining, respectively. *B*: Expression of Pdk1 in peritoneal macrophages and peripheral tissues. Western blot of Pdk1 and tubulin (loading control) in the white adipose tissue (WAT), liver, spleen, brown adipose tissue (BAT), lungs, heart, and kidneys of control and *LysMPdk1*$^{-/-}$ (KO) mice. *C*: The percentages of nuclear Foxo1^{+} among F4/80^{+} cells in epididymal fat of control, *LysMPdk1*$^{-/-}$, and *Δ256LysMPdk1*$^{-/-}$ mice aged 20–24 weeks. Counting of cells stained with anti-F4/80 and anti-FOXO1 are described in RESEARCH DESIGN AND METHODS. Values are means + SEM of three mice in each genotype. *$P < 0.005$ (one-factor ANOVA). *D*: Body weight of control, *LysMPdk1*$^{-/-}$, and *Δ256LysMPdk1*$^{-/-}$ fed an NCD. Data are means + SEM of 18–20 mice in each genotype. *E*: IPGTT of control (open circle), *LysMPdk1*$^{-/-}$ (red circle), and *Δ256LysMPdk1*$^{-/-}$ (blue circle) mice fed an NCD. Data are means + SEM of 20–25 mice in each genotype at age 20–24 weeks. *$P < 0.05$ (two-way repeated-measures ANOVA with an ad hoc multiple comparison method [Fisher LSD test] of *LysMPdk1*$^{-/-}$ vs. control or *Δ256LysMPdk1*$^{-/-}$ mice). *F*: Comparison of AUC in control, *LysMPdk1*$^{-/-}$, and *Δ256LysMPdk1*$^{-/-}$ mice during IPGTT. Data are means + SEM of 20–25 mice in each genotype. *$P < 0.01$ (two-way repeated-measures ANOVA with Fisher LSD test of *LysMPdk1*$^{-/-}$ vs. *Δ256LysMPdk1*$^{-/-}$ mice) and **$P < 0.05$ (two-way repeated-measures ANOVA with Fisher LSD test of *LysMPdk1*$^{-/-}$ vs. control mice). *G* and *H*: Insulin secretion (*G*) of control (open circle), *LysMPdk1*$^{-/-}$ (red circle), and *Δ256LysMPdk1*$^{-/-}$ (blue circle) mice during IPGTT and blood glucose (H) during ITT. Data are

R26$^{floxneo\Delta256FoxO1}$ (11) with *LysMCre* transgenic mice to generate *R26*$^{floxneo\Delta256FoxO1}$ *LysMCre* (*Δ256Foxo1*^{LysM}) double heterozygotes. Real-time PCR analysis and immunofluorescence confirmed the macrophage-specific expression of the transgene and the nuclear localization of FLAG-Δ256Foxo1, respectively (Supplementary Figs. 1 and 2). We crossed *Δ256Foxo1*^{LysM} with *Pdk1*$^{flox/+}$ to generate double mutant mice (*Δ256Foxo1*^{LysM}*Pdk1*$^{+/-}$). Finally, these mice were crossed with *Pdk1*$^{flox/+}$ to generate *Δ256Foxo1*^{LysM}*Pdk1*$^{-/-}$ (*Δ256LysMPdk1*$^{-/-}$) mice (Supplementary Fig. 3). As expected, *Δ256LysMPdk1*$^{-/-}$ mice showed excess nuclear Foxo1 in F4/80$^+$ cells from epididymal fat (Fig. 2*C*).

The *LysMPdk1*$^{-/-}$ and *Δ256LysMPdk1*$^{-/-}$ mice exhibited normal body weight when fed an NCD (Fig. 2*D*), and their epididymal fat tissue weight and adipocyte sizes were similar to those of control mice (Supplementary Fig. 4*A* and *B*). However, the IPGTTs revealed that *LysMPdk1*$^{-/-}$, but not *Δ256LysMPdk1*$^{-/-}$, mice exhibited glucose intolerance (Fig. 2*E* and *F*). Insulin secretion during the IPGTT was higher in *LysMPdk1*$^{-/-}$ mice than in controls and *Δ256LysMPdk1*$^{-/-}$ mice, but the difference was not significant (Fig. 2*G*). Furthermore, insulin tolerance significantly decreased in *LysMPdk1*$^{-/-}$ mice compared with control and *Δ256LysMPdk1*$^{-/-}$ mice (Fig. 2*H*). These data indicate that the deletion of *Pdk1* deteriorates insulin sensitivity and that the ectopic expression of Δ256Foxo1 ameliorates insulin sensitivity.

To identify the tissues that are responsible for insulin resistance, we investigated insulin-stimulated phosphorylation of IRS1, IRS2, and/or Akt in epididymal fats, liver, and skeletal muscle from control, *LysMPdk1*$^{-/-}$, and *Δ256LysMPdk1*$^{-/-}$ mice. In epididymal fat and liver, insulin-stimulated phosphorylation of IRS1 or IRS2 and Akt was significantly decreased in *LysMPdk1*$^{-/-}$ mice compared with control mice (Fig. 2*I*). However, insulin-stimulated phosphorylation of IRS and Akt in epididymal fat and liver from *Δ256LysMPdk1*$^{-/-}$ mice was similar to that of control mice (Fig. 2*I*). The expression of *G6pc* was significantly increased in liver from *LysMPdk1*$^{-/-}$ compared with *Δ256LysMPdk1*$^{-/-}$ mice (Fig. 2*J*); moreover, the hepatic glycogen content of *LysMPdk1*$^{-/-}$ mice was significantly decreased compared with control and *Δ256LysMPdk1*$^{-/-}$ mice (Fig. 2*K*). In contrast, Akt phosphorylation in skeletal muscle from *LysMPdk1*$^{-/-}$ mice was similar to that of control and *Δ256LysMPdk1*$^{-/-}$ mice (Fig. 2*I*). These data indicate that the deletion of *Pdk1* in ATMs led to insulin resistance, mainly in adipose tissue and liver, and that ectopic expression of Δ256Foxo1 ameliorated insulin resistance in those tissues.

Deletion of Pdk1 caused an increase of M1 macrophages in adipose tissues. A CLS is the accumulation of immune cells around dead adipocytes (32). We found that the number of F4/80$^+$ CLSs per field in epididymal fat was significantly higher in *LysMPdk1*$^{-/-}$mice than in control and *Δ256LysMPdk1*$^{-/-}$ mice (Fig. 3*A*).

The SVF of adipose tissue from 20-week-old mice contained a substantially higher proportion of F4/80$^+$ cells in *LysMPdk1*$^{-/-}$ compared with control mice (Fig. 3*B* and *C*). Analysis of macrophage subpopulations in the SVF showed a higher proportion of F4/80$^+$CD11c$^+$CD206$^-$ cells in *LysMPdk1*$^{-/-}$ mice than in control mice (Fig. 3*B* and *C*). In contrast, the adipose tissue of *Δ256LysMPdk1*$^{-/-}$ mice showed significantly reduced proportions of F4/80$^+$ cells and F4/80$^+$CD11c$^+$CD206$^-$ cells compared with *LysMPdk1*$^{-/-}$ mice (Fig. 3*B* and *C*). These data suggest that the deletion of *Pdk1* caused a significant increase in the proportion of M1 macrophages in epididymal fat, and the proportion was reduced with the overexpression of Δ256Foxo1.

Consistent with the above findings, the expression of chemokine (C-C motif) ligand 2 (*Ccl2*) (also known as monocyte chemoattractant protein-1 [*Mcp-1*]) and *Cd68* in epididymal fat (Fig. 3*D*) and of *Ccr2* and *Tnfa* in SVF from *LysMPdk1*$^{-/-}$ mice were significantly increased compared with control and *Δ256LysMPdk1*$^{-/-}$ mice (Fig. 3*E*). Furthermore, the expression level of IL-1 receptor antagonist, which is a naturally occurring antagonist of IL-1β and produced by adipose and other tissues (33), in SVF from *LysMPdk1*$^{-/-}$ mice was significantly decreased compared with control mice (Fig. 3*E*). These data support the notion that the deletion of *Pdk1* increased the recruitment of M1 macrophages to adipose tissues.

Macrophage-specific CNFoxo1 transgenic (*CNFoxo1*^{LysM}) mice exhibited insulin resistance. To clarify the function of Foxo1 in ATMs, we generated macrophage-specific CNFoxo1 transgenic mice. We crossed *Rosa26-CNFoxo1* (11) with *LysMCre* (*CNFoxo1*^{LysM}) mice. Real-time PCR revealed that the transgene was expressed exclusively in the spleen, liver, hypothalamus, and lung and in ATMs from the epididymal fat (Supplementary Fig. 5). These tissues have tissue-specific macrophages, which include the cells in the sinusoidal lining of the spleen, Kupffer cells in the liver, microglia in the hypothalamus, and alveolar macrophages in the lung (14,34,35). Therefore, resident macrophages likely account for the increased expression of the transgene in these tissues. Immunofluorescence of the epididymal fat showed that FLAG-CNFoxo1 was exclusively localized in the nucleus of F4/80$^+$ macrophages (Supplementary Fig. 6). Furthermore, immunofluorescence revealed that ~50% of F4/80$^+$ cells in epididymal fat of *CNFoxo1*^{LysM} mice were positive for FLAG (Fig. 4*A*) and that the percentages of nuclear Foxo1$^+$ cells in adipose tissue of *CNFoxo1*^{LysM} fed an HFD for 16 weeks was significantly increased compared with control mice fed an HFD or *CNFoxo1*^{LysM} fed an NCD (Fig. 4*B*). These results show that *CNFoxo1*^{LysM} mice were an appropriate model for studying the specific effects of overexpressing Foxo1 in ATMs.

On an NCD, *CNFoxo1*^{LysM} mice exhibited normal body weight, glucose tolerance, insulin secretion, and insulin sensitivity (Supplementary Fig. 7*A–D*). On an HFD, the body

means + SEM of 20–25 mice in each genotype. *$P < 0.05$ (two-way repeated-measures ANOVA with Fisher LSD test of control vs. *LysMPdk1*$^{-/-}$ or *Δ256LysMPdk1*$^{-/-}$ mice). *I*: Insulin-stimulated phosphorylation of IRSs and Akt in epididymal fat (WAT), liver, and skeletal muscle from control, *LysMPdk1*$^{-/-}$, and *Δ256LysMPdk1*$^{-/-}$ mice in the random fed state. Values were normalized to β-actin expression and represent means + SEM of 8–10 mice in each genotype. *$P < 0.05$ (one-factor ANOVA of *LysMPdk1*$^{-/-}$ vs. *Δ256LysMPdk1*$^{-/-}$). *K*: Hepatic glycogen content. Control ($n = 9$), *LysMPdk1*$^{-/-}$ ($n = 9$), and *Δ256LysMPdk1*$^{-/-}$ ($n = 8$) mice were killed in the random fed state for the determination of glycogen levels in liver extracts. Data are means + SEM of hepatic glycogen content corrected by the weight of liver per genotype. *$P < 0.05$ (one-factor ANOVA of control vs. *LysMPdk1*$^{-/-}$ mice). (A high-quality digital representation of this figure is available in the online issue.)

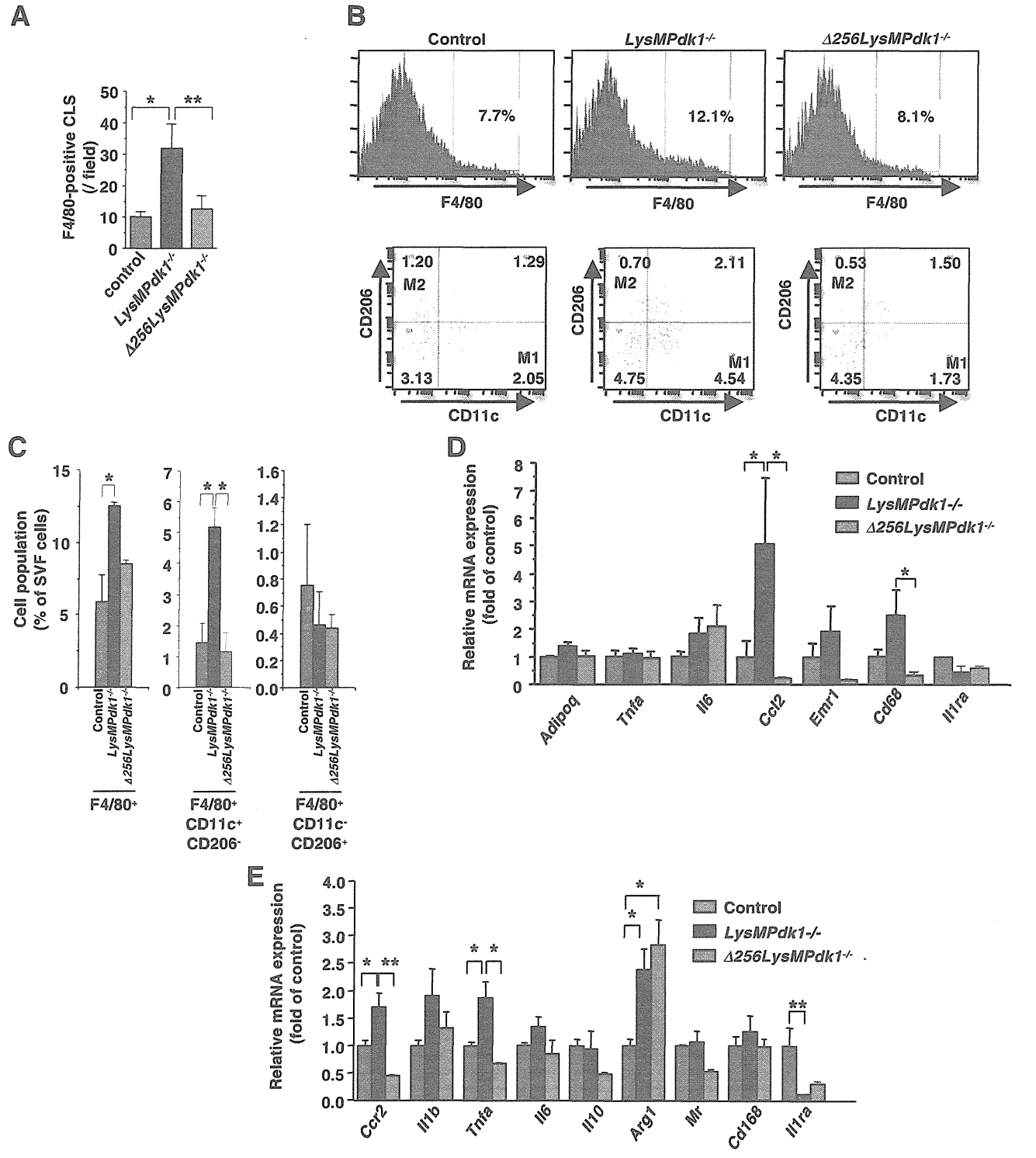

FIG. 3. Effects of *Pdk1* deletion or inhibition of the transactivation of Foxo1 on adipose tissue inflammation. *A*: CLSs in epididymal fats were quantified from eight different fields per mouse and presented as number of CLSs per field. Data are means + SEM of 9–10 mice in each genotype. $^*P < 0.01$ (one-factor ANOVA of *LysMPdk1*$^{-/-}$ vs. control mice) and $^{**}P < 0.05$ (one-factor ANOVA of *LysMPdk1*$^{-/-}$ vs. *Δ256LysMPdk1*$^{-/-}$ mice). *B*: The expression of F4/80 and CD11c and CD206 in the SVF of epididymal fat from 20- to 24-week-old mice of the indicated genotype as assessed by flow cytometry. *C*: The percentages of F4/80$^+$, F4/80$^+$CD11c$^+$CD206$^-$, and F4/80$^+$CD11c$^-$CD206$^+$ cells within the viable SVF from 20- to 24-week-old mice of control, *LysMPdk1*$^{-/-}$, and *Δ256LysMPdk1*$^{-/-}$ mice. Data are means + SEM of three mice in each genotype analyzed in three independent experiments. $^*P < 0.05$ (one-factor ANOVA of *LysMPdk1*$^{-/-}$ vs. control or *Δ256LysMPdk1*$^{-/-}$ mice). *D*: Expression of genes in the epididymal fat of control, *LysMPdk1*$^{-/-}$, and *Δ256LysMPdk1*$^{-/-}$ mice. Values were normalized to β-actin expression and represent the means + SEM of 8–10 mice per genotype. $^*P < 0.05$ (one-factor ANOVA). *E*: Expression of genes specific for M1 (*Ccr2*, *Il1b*, *Tnfa*, and *Il6*) or M2 (*Il10*, *Arg1*, *Mr*, and *Cd168*) macrophage in SVF of epididymal fat in control, *LysMPdk1*$^{-/-}$, and *Δ256LysMPdk1*$^{-/-}$ mice. Values were normalized to β-actin expression and represent the means + SEM of 8–10 mice per genotype. $^*P < 0.05$ and $^{**}P < 0.01$ (one-factor ANOVA).

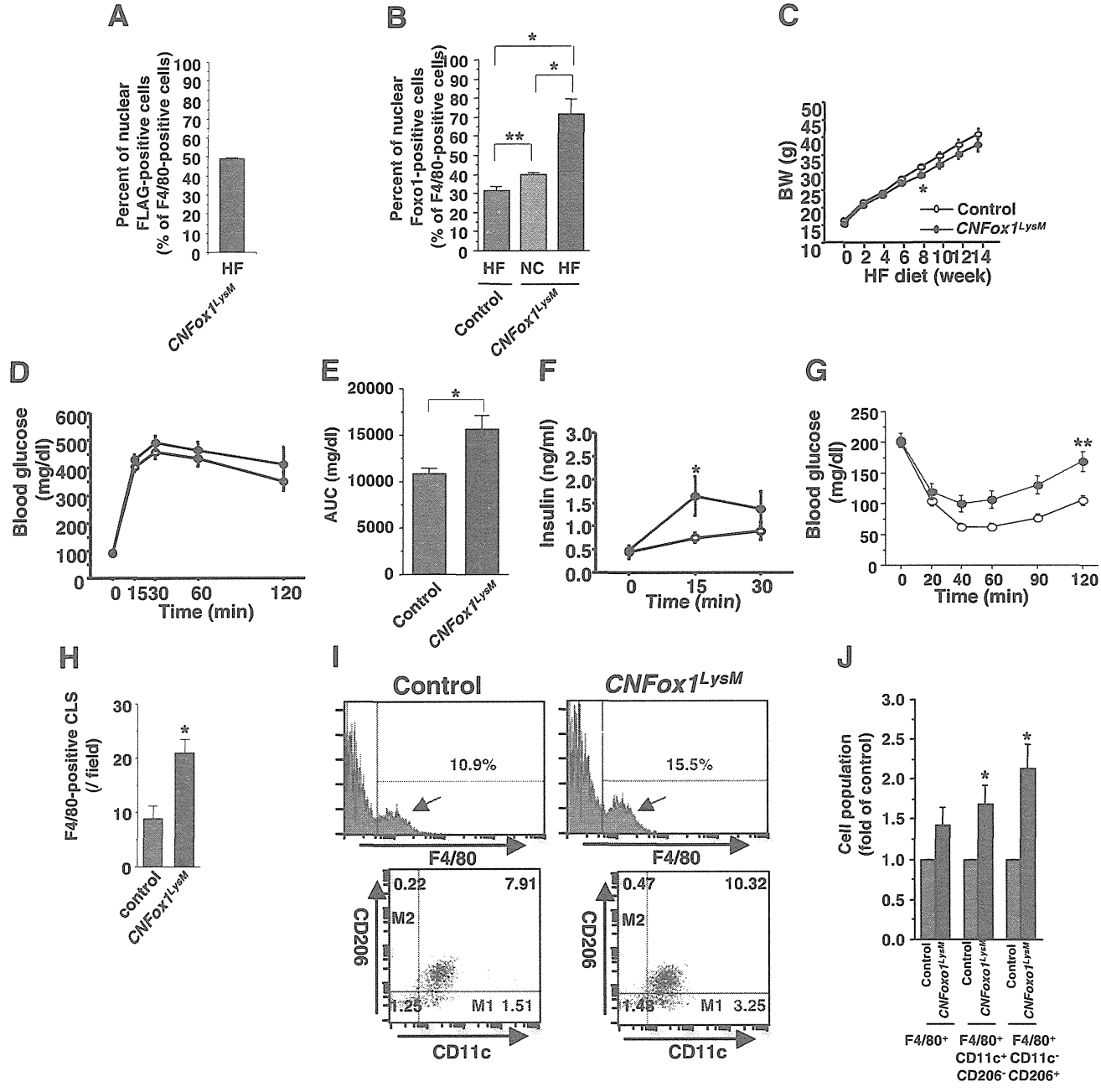

FIG. 4. Effects of the overexpression of CNFoxo1 in macrophages on glucose metabolism and adipose tissue inflammation. *A*: The percentages of nuclear FLAG$^+$ among F4/80$^+$ cells in epididymal fat of *CNFoxo1*^{LysM} fed an HFD for 16 weeks. Counting of cells stained with anti-FLAG and anti-F4/80 are described in RESEARCH DESIGN AND METHODS. *B*: The percentages of nuclear Foxo1$^+$ among F4/80$^+$ cells in epididymal fat of control, *CNFoxo1*^{LysM} fed an NC, and *CNFoxo1*^{LysM} mice aged 20 weeks and fed an HFD for 16 weeks. Counting of cells stained with anti-F4/80 and anti-FOXO1 are described in RESEARCH DESIGN AND METHODS. Values are means + SEM of eight mice in each genotype. *$P < 0.005$ and **$P < 0.05$ (one-factor ANOVA). *C*: Body weight (BW) of control and *CNFoxo1*^{LysM} mice fed an HFD. Data are means + SEM of 18–20 mice in each genotype. *$P < 0.05$ (two-way repeated-measures ANOVA with an ad hoc multiple comparison method [Fisher LSD test] of control vs. *CNFoxo1*^{LysM} mice after 8 weeks of HFD). *D*: IPGTT of control (open circle) and *CNFoxo1*^{LysM} (blue circle) mice fed an HFD. Data are means + SEM of 20–25 mice in each genotype. *E*: Comparison of AUC in control and *CNFoxo1*^{LysM} mice during IPGTT. Data are means + SEM of 20–25 mice in each genotype. *$P < 0.05$ (two-way repeated-measures ANOVA with Fisher LSD test of control vs. *CNFoxo1*^{LysM} mice). *F*: Insulin secretion of control (open circle) and *CNFoxo1*^{LysM} (blue circle) mice during IPGTT. Data are means + SEM of 20–25 mice in each genotype. *$P < 0.05$ (two-way repeated-measures ANOVA with Fisher LSD test of control vs. *CNFoxo1*^{LysM} mice). *G*: ITT of control (open circle) and *CNFoxo1*^{LysM} (blue circle) mice. Data are means + SEM of 20–25 mice in each genotype. *$P < 0.01$ and **$P < 0.05$ (two-way repeated-measures ANOVA with Fisher LSD test of control vs. *CNFoxo1*^{LysM} mice). *H*: CLSs in epididymal fats were quantified from eight different fields per mouse and presented as number of CLSs per field. Data are means + SEM of 9–10 mice in each genotype. *$P < 0.05$ (one-factor ANOVA of control vs. *CNFoxo1*^{LysM} mice). *I*: Expression of F4/80 and CD11c and CD206 in cells of the SVF of epididymal fat from control and *CNFoxo1*^{LysM} mice fed an HFD for 16 weeks as assessed by flow cytometry. *J*: The percentages of F4/80$^+$, F4/80$^+$CD11c$^+$CD206$^-$, and F4/80$^+$CD11c$^-$CD206$^+$ cells within the viable SVF from control and *CNFoxo1*^{LysM} 20- to 24-week-old mice fed an HFD for 16 weeks. The percentages of cell population among total SVF cells were calculated in each experiment. Data are means + SEM of fold change of control mice in each genotype ($n = 3$) analyzed in three independent experiments. *$P < 0.05$ (one-factor ANOVA of control vs. *CNFoxo1*^{LysM} mice).

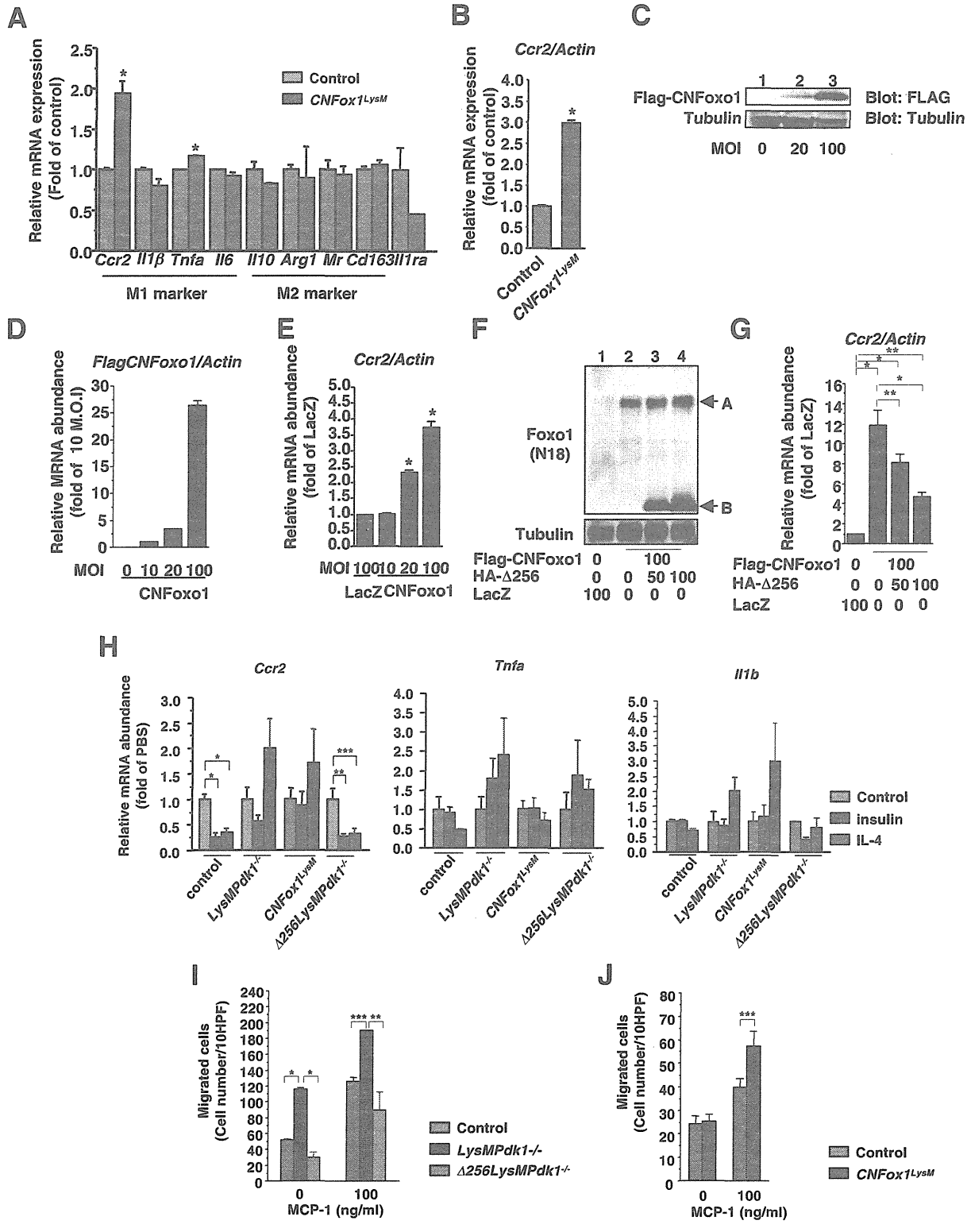

FIG. 5. Foxo1 increases migration capacity by inducing *Ccr2* expression. *A*: Expression of genes specific for M1 (*Ccr2*, *Il1b*, *Tnfa*, and *Il6*) or M2 (*Il10*, *Arg1*, *Mr*, and *Cd168*) phenotype of cells of the SVF from control and *CNFoxo1*^{LysM} mice fed an HFD for 16 weeks. Values were normalized to β-actin expression and represent the means + SEM of 8–10 mice per genotype. *$P < 0.05$ (one-factor ANOVA of control vs. *CNFoxo1*^{LysM} mice). *B*: Expression of *Ccr2* in ATMs sorted from the SVF of epididymal fat from control and *CNFoxo1*^{LysM} mice fed an HFD for 16 weeks. Values were normalized to β-actin expression and represent the means + SEM of three mice per genotype. *$P < 0.05$ (one-factor ANOVA of control vs. *CNFoxo1*^{LysM} mice). *C*: Flag-CNFoxo1 protein expression was detected in RAW264.7 cells. Nontransduced RAW264.7 cells (*lane 1*); RAW264.7 cells transduced with adenovirus encoding CNFoxo1 at 20 and 100 MOI (*lanes 2* and *3*, respectively). Western blot of cell lysates using anti-tubulin antibody (*bottom*). *D*: Expression of *Flag-CNFoxo1* gene in RAW264.7 cells transduced with adenoviruses encoding CNFoxo1 at the indicated MOI. *E*: Real-time PCR to determine *Ccr2* expression in RAW264.7 cells transduced with adenovirus encoding LacZ or CNFoxO1 at the indicated

and tissue weights of *CNFoxo1*^{LysM} mice were similar to those of control mice. However, adipocyte size in the epididymal fat of *CNFoxo1*^{LysM} mice tended to be larger than that in control mice (Fig. 4*C* and Supplementary Fig. 8*A–C*). Although, on the HFD, *CNFoxo1*^{LysM} and control mice exhibited similar glucose tolerance (Fig. 4*D*), the AUC of the IPGTT was significantly increased in *CNFoxo1*^{LysM} compared with control mice (Fig. 4*E*). Furthermore, the *CNFoxo1*^{LysM} mice exhibited significantly increased insulin secretion and decreased insulin sensitivity (Fig. 4*F* and *G*). These data suggest that the CNFoxo1 in ATMs caused insulin resistance.

M1 macrophage population was increased in *CNFoxo1*^{LysM} mice. Adipocyte size and CLS density exhibit a positive correlation (32,36). Indeed, under HFD conditions, *CNFoxo1*^{LysM} mice had a significantly higher number of CLSs in epididymal fat than control mice (Fig. 4*H*). Phenotypic analysis of ATMs revealed significantly more F4/80$^+$ cells in the SVF of *CNFoxo1*^{LysM} mice compared with control mice (Fig. 4*I* and *J*). Further analysis showed that *CNFoxo1*^{LysM} mice had a significantly higher percentage of F4/80$^+$CD11c$^+$CD206$^-$ and F4/80$^+$CD11c$^-$CD206$^+$ cells compared with control mice (Fig. 4*I* and *J*). These data suggest that the *CNFoxo1*^{LysM} mice have increased numbers of macrophages in adipose tissues under HFD conditions.

CNFoxo1-induced *Ccr2* gene expression. To investigate how CNFoxo1 increased the M1 macrophage subpopulation in adipose tissue, we analyzed gene expression in the SVF of epididymal fat from mice fed an HFD. Real-time PCR demonstrated that *CNFoxo1*^{LysM} mice expressed significantly higher levels of *Ccr2* and *Tnfa* mRNAs than control mice (Fig. 5*A*). Furthermore, the level of *Ccr2* expression in F4/80$^+$CD11c$^+$CD206$^-$ cells was significantly increased in *CNFoxo1*^{LysM} mice compared with control mice (Fig. 5*B*). To examine whether CNFoxo1 directly induces *Ccr2* expression, we infected RAW264.7 cells with an adenovirus encoding β-galactosidase or CNFoxo1. Overexpression of CNFoxo1 in RAW264.7 cells significantly increased endogenous *Ccr2* expression (Fig. 5*C–E*). These data suggest that the overexpression of CNFoxo1 in ATMs increased *Ccr2* expression.

Next, we investigated whether Δ256Foxo1 could block Foxo1-induced *Ccr2* expression. We cotransduced RAW264.7 cells with adenoviruses that encoded Flag-CNFoxo1 and HA-Δ256Foxo1. We found that the presence of Δ256Foxo1 inhibited the expression of endogenous *Ccr2* in a dose-dependent manner (Fig. 5*F* and *G*). These data indicate and confirm that the Δ256Foxo1 construct had a dominant negative effect on Foxo1-induced *Ccr2* expression.

Insulin- and IL-4–inhibited *Ccr2* gene expression. To determine whether Foxo1 regulation of *Ccr2* expression was involved in insulin signaling, we tested whether insulin or IL-4 inhibited *Ccr2* expression in a Foxo1-dependent manner. Both insulin and IL-4 could significantly inhibit *Ccr2* expression in BMDMs from control and *Δ256LysMPdk1*$^{-/-}$ mice but not in BMDMs from *LysMPdk1*$^{-/-}$ and *CNFoxo1*^{LysM} mice (Fig. 5*H*). In contrast, insulin and IL-4 did not affect expression of other genes specifically expressed in M1 macrophages, including *Tnfa* and *Il1b* (Fig. 5*H*). These data indicate that Foxo1-induced *Ccr2* expression was regulated by both insulin and IL-4.

Pdk1 deletion or CNFoxo1 expression enhanced macrophage migration. To analyze the functional effects of Pdk1 deficiency in macrophages, we performed transwell migration assays with BMDMs. Pdk1-deficient BMDMs exhibited significantly more migration than BMDMs from control and *Δ256LysMPdk1*$^{-/-}$ mice (Fig. 5*I*). Furthermore, BMDMs from *CNFoxo1*^{LysM} mice exhibited significantly increased MCP-1–stimulated migration capacity compared with control BMDMs (Fig. 5*J*). These data confirm that a Pdk1 deficiency and/or Foxo1 activation in macrophages resulted in increased migration as a result of increased expression of Ccr2.

Characterization of the Foxo1 response element within the *Ccr2* promoter. To characterize the Foxo1 response element (FRE) in the *Ccr2* promoter, we constructed different versions of the mouse *Ccr2* promoter by progressively deleting portions of the upstream region. The transcriptional activity of each mutant promoter in response to CNFoxo1 binding was examined in HEK293T cells (Fig. 6*A*). *Ccr2* promoters with deletions up to −291 nucleotides (nt) responded to Foxo1 transactivation. However, further deletions, up to −208 nt, completely abolished transcription of the reporter (Fig. 6*A*). Thus, the FRE was confined to a small nucleotide region between −291 and −208 in the mouse *Ccr2* promoter. Consistent with this observation, the promoter region contained several putative Foxo response elements (FREs), including GTAAAT from −254 to −249 nt and AAACA from −215 to −211 nt (Fig. 6*A*). It is interesting that the former region is conserved among human, mouse, and rat *Ccr2* promoters (Supplementary Fig. 9). To confirm this finding, we generated one additional truncated mutant promoter (237Ccr2), which had the latter FRE but not the former. The 237*Ccr2* promoter did not respond to Foxo1 induction. These data suggest that the AAACA sequence from −215 to −211 was unnecessary for Foxo1 activation of the *Ccr2* promoter. We also generated two additional mutant *Ccr2* promoters, one harboring nucleotide substitutions between −254 and −249 (254mut) and one with substitutions between −215 and −211 (215mut). Foxo1 induced transcription from the 215mut but not from the 254mut *Ccr2* promoter (Fig. 6*A*). These data suggest that the GTAAAT

MOI. The cells were transduced, incubated in complete medium, and harvested 48 h after transduction. Data (mean ± SEM) are from three independent experiments and normalized to the amount of β-actin mRNA, expressed as relative to the corresponding LacZ value. *$P < 0.05$ (one-factor ANOVA of cells transduced with LacZ vs. CNFoxo1 at 20 or 100 MOI). *F*: Expression of Flag CNFoxO1 and HA-Δ256FoxO1 at indicated MOI in RAW264.7 cells. Western blot using anti-Foxo1 (N18) antibody, which recognizes the NH_2 terminus of Foxo1 (*top*). Arrows A and B indicate Flag-CNFoxo1 and HA-Δ256Foxo1, respectively. *G*: The effects of HA-Δ256Foxo1 on Flag-CNFoxo1–induced *Ccr2* expression in RAW264.7 cells. Data are means + SEM from three independent experiments and are expressed as the fold change from endogenous *Ccr2* expression in RAW264.7 cells transduced with an adenovirus encoding LacZ. *$P < 0.005$ and **$P < 0.05$ (one-factor ANOVA of cells transduced with LacZ vs. Flag-CNFoxo1 at MOI 100 and cells transduced with Flag-CNFoxo1 at MOI 100 vs. HA-Δ256Foxo1 at MOI 50 and 100). *H*: Expression of genes *Ccr2*, *Tnfa*, and *Il1b* of BMDM from the indicated genotypes. Cells were cultured for 6 days in the presence of PBS, insulin (100 nmol/L), or IL-4 (100 ng/mL). Values were normalized to β-actin expression and represent the means + SEM of fold of PBS in each genotype (8–10 mice per genotype). *$P < 0.005$ (one-factor ANOVA of PBS vs. insulin or IL-4 in control mice), **$P < 0.01$ (one-factor ANOVA of PBS vs. insulin in *Δ256LysMPdk1*$^{-/-}$ mice), and ***$P < 0.05$ (one-factor ANOVA of PBS vs. IL-4 in *Δ256LysMPdk1*$^{-/-}$ mice). *I* and *J*: Migration of BMDM from control, *LysMPdk1*$^{-/-}$, and *Δ256LysMPdk1*$^{-/-}$ mice (*I*) and from control and *CNFoxo1*^{LysM} mice (*J*) through a gelatin matrix was analyzed using a transwell migration assay at the indicated concentration of MCP-1. Data are means + SEM of cell numbers per 10 high power fields (HPFs) from three independent experiments. *$P < 0.005$ (one-factor ANOVA of *LysMPdk1*$^{-/-}$ vs. control or *Δ256LysMPdk1*$^{-/-}$ mice at basal condition), **$P < 0.01$ (one-factor ANOVA of *LysMPdk1*$^{-/-}$ vs. *Δ256LysMPdk1*$^{-/-}$ mice at 100 ng/mL of MCP-1), and ***$P < 0.05$ (one-factor ANOVA of *LysMPdk1*$^{-/-}$ vs. control mice and of control vs. *CNFoxo1*^{LysM} mice at 100 ng/mL of MCP-1).

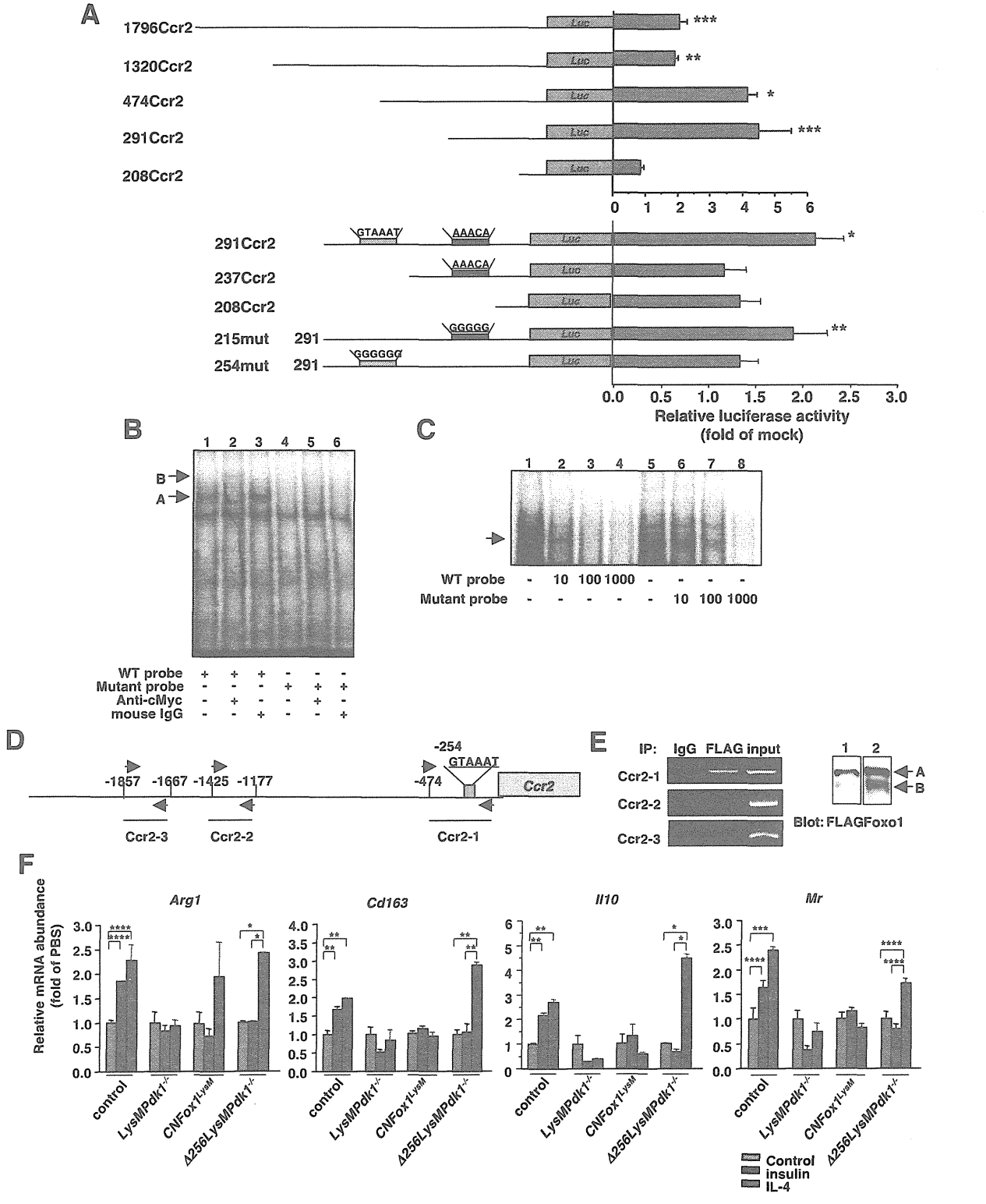

FIG. 6. *Ccr2* as a target gene of Foxo1 and the effects of insulin or IL-4 on genes for M2 signature. *A*: Effect of Foxo1 on Ccr2 promoter activity. Data were obtained from 10 experiments and are represented as means ± SEM of fold change from mock vector-transfected activity. $*P < 0.001$, $**P < 0.005$, and $***P < 0.05$ (one-factor ANOVA of cells transfected with pCMV5/cMyc and pCVM5/cMyc-CNFoxo1 vector). *B*: EMSA of Foxo1 binding to DNA. The DNA probe was derived from a 31–base pair DNA covering the consensus Foxo1 binding site (−267/−237 nt) of the mouse Ccr2 promoter (*lanes 1–3*). A mutant DNA with an altered Foxo1 binding motif was used as a control (*lanes 4–6*). The position of the slowed complex is indicated as A, and the supershifted complex is indicated as B. *C*: Oligonucleotide probes corresponding to the Foxo1 binding site of the *Ccr2* promoter were incubated with nuclear extracts in the absence or presence of increasing amounts of unlabeled wild-type (*lanes 1–4*) or mutant oligonucleotide (*lanes 5–8*). *D*: Mouse *Ccr2* promoter and primer pairs used in ChIP assay. The magenta box indicates a consensus Foxo1 binding site. *E*: ChIP assays of RAW264.7 cells transduced with an adenovirus encoding CNFoxo1 and harvested 36 h after transduction (*left*). The PCR primers amplified the mouse *Ccr2* promoter sequence as shown in Fig. 5*G*. PCR reactions with total input chromatin are shown as control.

sequence from −254 to −249 nt in the mouse *Ccr2* promoter was the functional FRE.

Association of Foxo1 with the *Ccr2* promoter. To examine the ability of this putative FRE to bind Foxo1, we conducted an EMSA. Foxo1 caused significant retardation of the FRE DNA (Fig. 6*B*, *lane 1*). Inclusion of the anti-cMyc antibody resulted in a supershifted DNA band (Fig. 6*B*, *lane 2*). The same EMSA was performed using a mutant DNA containing five base substitutions within the FRE motif as a control. Alterations in the consensus FRE motif abrogated its ability to bind Foxo1 (Fig. 6*B*, *lane 4*). Incubating nuclear extracts from cells expressing cMyc-tagged Foxo1 with a probe encoding the 31–base pair FRE DNA sequence yielded a slower complex that was competed out by excess cold probe (Fig. 6*C*, *lanes 1–4*) but not mutant probe (Fig. 6*C*, *lanes 5–8*).

We performed a ChIP assay to determine the association between Foxo1 and the *Ccr2* promoter in RAW264.7 cells. Because of low levels of Foxo1 expression in RAW264.7 cells, we transduced cells with adenovirus encoding CNFoxo1. Using primers flanking the FRE motif within the *Ccr2* promoter (Fig. 6*D*), we detected a sequence-specific DNA corresponding to the proximal region (−474/9 nt) of the *Ccr2* promoter in immunoprecipitates obtained with anti-FLAG antibody (Fig. 6*E*). We also performed PCR analysis using a pair of off-target primers flanking distal regions (−1857/−1667 and −1425/−1177 nt). No specific DNA was amplified in the immunoprecipitates using normal mouse IgG or anti-FLAG antibody (Fig. 6*E*). These data confirm that Foxo1 directly binds the *Ccr2* promoter and that *Ccr2* is a target gene of Foxo1.

The Pdk1-Foxo1 pathway plays a role in alternative macrophage activation. To determine whether the Pdk1-Foxo1 pathway was essential for alternative activation of macrophages, we analyzed macrophage signatures in insulin- or IL-4–stimulated BMDMs from control, *LysMPdk1*$^{-/-}$, *CNFoxo1*^{LysM}, and *Δ256LysMPdk1*$^{-/-}$ mice. The signature genes, including *Arg1*, *Cd163*, *Il10*, and *Mr*, were significantly induced by insulin or IL-4 in BMDMs from control mice (Fig. 6*F*). In contrast, Pdk1 deficiency or constitutive Foxo1 activation completely abolished insulin- or IL-4–stimulated induction of the genes necessary for alternative macrophage activation (Fig. 6*F*). It is interesting that the expression of transactivation-defective (Δ256) Foxo1 rescued IL-4–induced, but not insulin-induced, gene expression (Fig. 6*F*). These data indicate that the Pdk1-Foxo1 pathway was required for the activation of macrophages via the alternative pathway.

A transactivation-defective (Δ256) Foxo1 partially protected against diet-induced insulin resistance. To determine whether blocking Foxo1 transactivation by expressing Δ256Foxo1 in ATMs would alleviate insulin resistance, we compared glucose homeostasis and insulin sensitivity in wild-type and *Δ256Foxo1*^{LysM} mice fed an HFD for 24 weeks. We observed no differences in body weight, glucose tolerance, or insulin secretion between genotypes (Fig. 7*A–C*). Furthermore, the *Δ256Foxo1*^{LysM} mice showed a weak but significant improvement in insulin sensitivity compared with wild-type mice (Fig. 7*D* and *E*).

After a 24-week HFD, *Δ256Foxo1*^{LysM} and wild-type mice had similar proportions of F4/80$^+$, F4/80$^+$CD11c$^+$CD206$^-$, and F4/80$^+$CD11c$^-$CD206$^+$ cells in adipose tissues (Fig. 7*F*). Moreover, in epididymal fat, no differences were observed in the gene expression profiles of M1 macrophages, including *Ccr2*, *Il1b*, *Tnfα*, and *Il6*. However, there was a significant increase in *Arg1* expression in *Δ256Foxo1*^{LysM} compared with control mice (Fig. 7*G*). Taken together, these data show that overexpression of Δ256Foxo1 in macrophages did not prevent glucose intolerance, but it did partially alleviate insulin resistance.

DISCUSSION

In the current study, we demonstrate that Pdk1 in ATMs inhibits recruitment of M1 macrophages into adipose tissues, while Foxo1 antagonizes these processes. These findings suggest that the Pdk1-Foxo1 signaling pathway in ATMs is important for regulation of chronic inflammation and insulin sensitivity in vivo (Fig. 8).

The key finding of the current study was that Foxo1 targeted *Ccr2* expression in macrophages. Ccr2 is the primary receptor for Mcp1/Ccl2, a member of the chemokine family of proteins. Ccr2 is expressed on circulating monocytes and ATMs, where it serves as a crucial monocyte recruitment factor by directing macrophages to sites of injury and inflammation. Furthermore, Ccr2 is important in the regulation of insulin sensitivity in vivo. Obesity increases the production of Ccl2 in adipose tissues, which leads to an accumulation of Ccl2-bound macrophages. When recruited macrophages are classically activated, they secrete proinflammatory cytokines, which leads to insulin resistance in various insulin-responsive tissues (2). Indeed, *Ccr2* deletion ameliorated insulin resistance in HFD-induced insulin resistance (37). Therefore, our observation of increased *Ccr2* expression in SVF M1 macrophages in *LysMPdk1*$^{-/-}$ and *CNFoxo1*^{LysM} mice was an important cue that insulin resistance had developed. Thus, the current study directly demonstrates that ATM Foxo1 played a pivotal role in regulating insulin sensitivity in vivo.

Nuclear accumulation of Foxo1 suddenly increased at 24 weeks of HFD, although phosphorylation of Pdk1 was not changed. These findings suggest that another signaling pathway may be involved in subcellular localization of Foxo1 in ATMs. One of the candidates is MST1, which mediates oxidative stress, phosphorylates FOXO proteins at a conserved site within the forkhead domain, disrupts their interaction with 14-3-3 proteins, and promotes FOXO nuclear translocation (27). Furthermore, JNK is known to phosphorylate and activate MST1 (30). HFD increased oxidative stress (18), leading to activation of JNK, MST1, and nuclear accumulation of Foxo1 (27). Of interest, we observed that H_2O_2 significantly increased at 24 weeks of HFD and that phosphorylation of MST1 also significantly increased at the same time. Therefore, oxidative stress in HFD may contribute to nuclear accumulation and activation of Foxo1. The findings suggest that nuclear accumulation of Foxo1 contributes to recruitment of M1 macrophages into adipose tissue during HFD.

Western blotting of transduced CNFoxo1 using anti-FLAG (*lane 1*) and anti-Foxo1 (*lane 2*) antibodies (*right*). The position of CNFoxo1 is indicated as A, and endogenous Foxo1 is indicated as B. *F*: Expression of genes *Arg1*, *Cd163*, *Il10*, and *Mr* of BMDM from the indicated genotypes. Cells were cultured for 2 days in the presence of PBS (control), insulin (100 nmol/L), or IL-4 (100 ng/mL). Values were normalized to β-actin expression and represent the means + SEM of fold of PBS in each genotype (8–10 mice per genotype). *P < 0.001, **P < 0.005, ***P < 0.01, and ****P < 0.05 (one-factor ANOVA among the indicated genotypes). WT, wild-type.

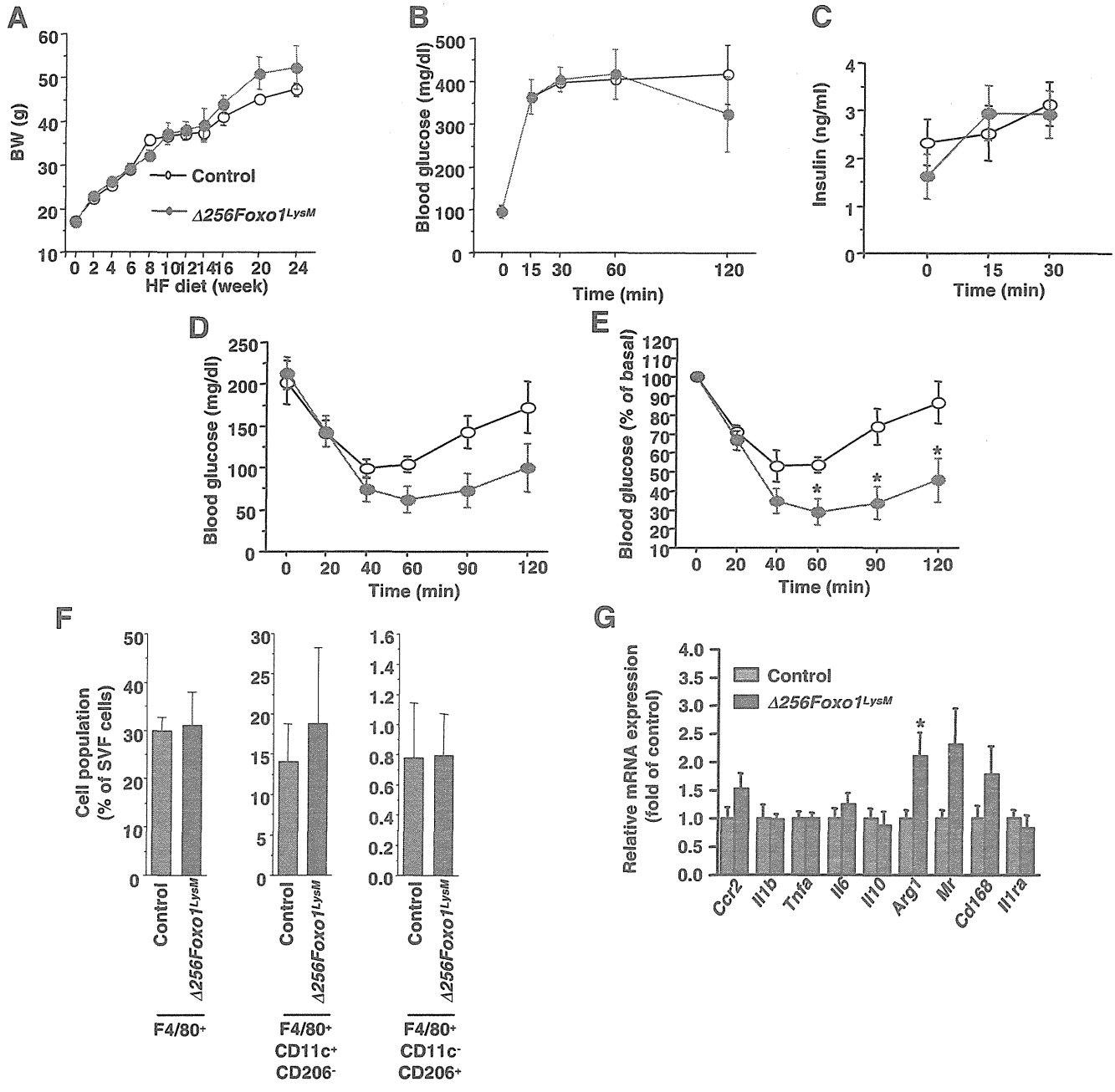

FIG. 7. A transactivation-defective (Δ256) Foxo1 partially protected against diet-induced insulin resistance. *A*: Body weight (BW) of control and *Δ256Foxo1*^{LysM} mice fed an HFD. Data are means + SEM of 20 mice in each genotype. *B*: IPGTT of control (open circle) and *Δ256Foxo1*^{LysM} (magenta circle) mice fed an HFD. Data are means + SEM of 20 mice in each genotype. *C*: Insulin secretion of control (open circle) and *Δ256Foxo1*^{LysM} (magenta circle) mice during IPGTT. Data are means + SEM of 20 mice in each genotype. *D* and *E*: ITT of control (open circle) and *Δ256Foxo1*^{LysM} (magenta circle) mice. Data are means + SEM of 20 mice in each genotype as absolute glucose values (*D*) and the percentages of basal values (*E*). *$P < 0.05$ (two-way repeated-measures ANOVA with an ad hoc multiple comparison method [Fisher's LSD test] of control vs. *Δ256Foxo1*^{LysM} mice). *F*: The percentages of F4/80$^+$, F4/80$^+$CD11c$^+$CD206$^-$, and F4/80$^+$CD11c$^-$CD206$^+$ cells within the viable SVF from 20- to 24-week-old mice of control and *Δ256Foxo1*^{LysM} mice. Data are means + SEM of 6 mice in each genotype analyzed in three independent experiments. *G*: Expression of genes in the epididymal fat of control and *Δ256Foxo1*^{LysM} mice. Values were normalized to β-actin expression and represent the means + SEM of 8–10 mice per genotype. *$P < 0.05$ (one-factor ANOVA of control vs. *Δ256Foxo1*^{LysM} mice).

However, we observed that expression of Δ256Foxo1 just partially protected against diet-induced insulin resistance and could not rescue *Ccr2* expression in mice fed an HFD for 24 weeks. Furthermore, the current study demonstrates that nuclear localization of Foxo1 started to occur at 24 weeks of HFD. Therefore, it is possible that nuclear localization of Foxo1 plays a role specifically in the late progression of diet-induced insulin resistance. From the current study, nuclear accumulation of Foxo1 in ATMs is only 40–45% of all F4/80$^+$ at 24 weeks of HFD, which means that an HFD cannot activate Foxo1 in ATMs completely. In contrast, the percentages of nuclear Foxo1 in ATMs of *LysMPdk1*$^{-/-}$ and *CNFoxo1*^{LysM} fed an HFD are ~70%. Therefore, the effect of loss of transactivation of Foxo1 on *Ccr2* expression in an

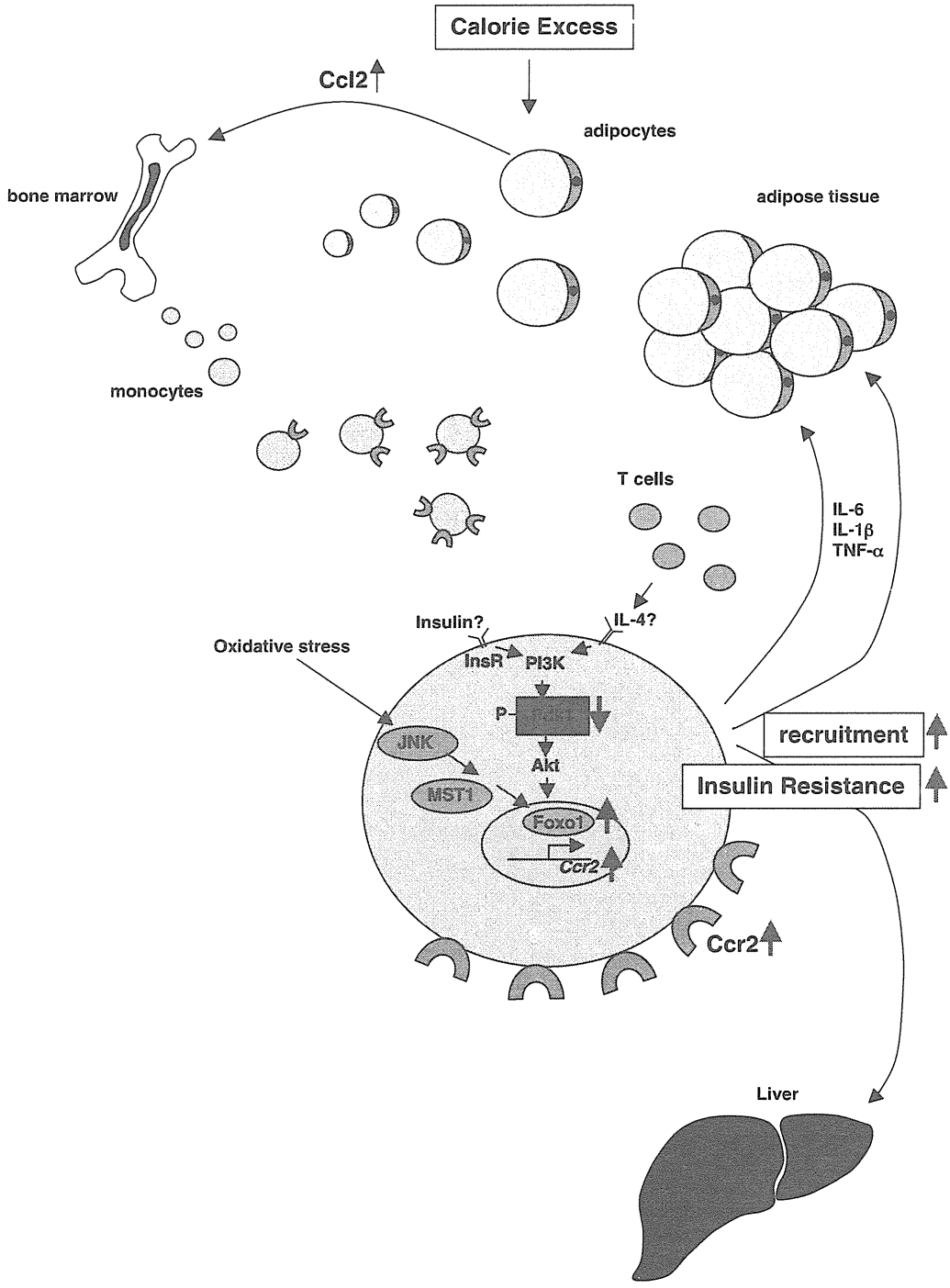

FIG. 8. Control of ATM function by Pdk1-Foxo1 pathway. Pdk1 is regulated by not only insulin but also cytokines, including IL-4, which is secreted from CD4$^+$ T cells or regulatory T cells. Furthermore, Foxo1 is regulated by not only Pdk1 but also oxidative stress through JNK and MST1. Phosphorylation of Pdk1 gradually declined during the HFD, but oxidative stress suddenly increased at the prolonged HFD, which is consistent with the time for the increased nuclear accumulation of Foxo1 in ATMs. Foxo1 directly regulates the expression of Ccr2, which upregulates the recruitment of macrophages in adipose tissue. PI3K, phosphatidylinositol 3-kinase.

HFD is small compared with *LysMPdk1*$^{-/-}$ mice. Alternatively, nuclear Foxo1 in myeloid cells may promote insulin resistance by other mechanisms than its role in the control of *Ccr2* gene expression. Furthermore, the *CNFoxo1*^{LysM} mice fed an NCD did not exhibit insulin resistance, while *LysMPdk1*$^{-/-}$ mice exhibited insulin resistance. These findings suggest that Foxo1 per se is not sufficient to cause HFD-induced insulin resistance, although Foxo1 may enhance the negative effect of an HFD on insulin sensitivity.

Our results provide direct evidence for the notion that ATM cell autonomous Pdk1-Foxo1 signaling regulates adipose tissue inflammation and insulin sensitivity in vivo. This finding may suggest a new target for pharmacological

intervention that could lead to novel therapeutic strategies for treating insulin resistance and type 2 diabetes.

ACKNOWLEDGMENTS

This work was supported by a grant from Nippon Boehringer Ingelheim Co., Ltd. to H.I. and a grant from Keio University Grant-in-Aid for Encouragement of Young Medical Scientists to Y.K. No other potential conflicts of interest relevant to this article were reported.

Y.K. researched data. J.N. conceived the hypothesis, designed and researched data, supervised the analyses, and wrote the manuscript. N.W., S.F., K.I., R.S., Y.H., and K.T. researched data. M.K. and T.N. generated and provided tissue-specific *Pdk1* knockout mice. A.Y. provided *LysMCre* mice and helpful discussion regarding experiments. M.O. researched data and assisted with data interpretation. H.I. supervised all experiments and assisted with preparation of the manuscript. J.N. is the guarantor of this work and, as such, had full access to all the data in the study and takes responsibility for the integrity of the data and the accuracy of the data analysis.

The authors thank Takahito Kaji (Training Department, Customer & Commercial Excellence, MSD K.K.) for analysis of data by two-way repeated-measures ANOVA.

REFERENCES

1. Qatanani M, Lazar MA. Mechanisms of obesity-associated insulin resistance: many choices on the menu. Genes Dev 2007;21:1443–1455
2. Olefsky JM, Glass CK. Macrophages, inflammation, and insulin resistance. Annu Rev Physiol 2010;72:219–246
3. Saltiel AR, Kahn CR. Insulin signalling and the regulation of glucose and lipid metabolism. Nature 2001;414:799–806
4. Welham MJ, Bone H, Levings M, et al. Insulin receptor substrate-2 is the major 170-kDa protein phosphorylated on tyrosine in response to cytokines in murine lymphohemopoietic cells. J Biol Chem 1997;272:1377–1381
5. Frittitta L, Grasso G, Munguira ME, Vigneri R, Trischitta V. Insulin receptor tyrosine kinase activity is reduced in monocytes from non-obese normoglycaemic insulin-resistant subjects. Diabetologia 1993;36:1163–1167
6. Zoppini G, Galante P, Zardini M, Muggeo M. Phosphotyrosine protein profiles in monocytes after insulin and IGF-1 stimulation. Eur J Clin Invest 1994;24:275–278
7. Liang CP, Han S, Okamoto H, et al. Increased CD36 protein as a response to defective insulin signaling in macrophages. J Clin Invest 2004;113:764–773
8. Han S, Liang CP, DeVries-Seimon T, et al. Macrophage insulin receptor deficiency increases ER stress-induced apoptosis and necrotic core formation in advanced atherosclerotic lesions. Cell Metab 2006;3:257–266
9. Senokuchi T, Liang CP, Seimon TA, et al. Forkhead transcription factors (FoxOs) promote apoptosis of insulin-resistant macrophages during cholesterol-induced endoplasmic reticulum stress. Diabetes 2008;57:2967–2976
10. Hashimoto N, Kido Y, Uchida T, et al. Ablation of PDK1 in pancreatic beta cells induces diabetes as a result of loss of beta cell mass. Nat Genet 2006;38:589–593
11. Iskandar K, Cao Y, Hayashi Y, et al. PDK-1/FoxO1 pathway in POMC neurons regulates Pomc expression and food intake. Am J Physiol Endocrinol Metab 2010;298:E787–E798
12. Su D, Coudriet GM, Hyun Kim D, et al. FoxO1 links insulin resistance to proinflammatory cytokine IL-1beta production in macrophages. Diabetes 2009;58:2624–2633
13. Fan W, Morinaga H, Kim JJ, et al. FoxO1 regulates Tlr4 inflammatory pathway signalling in macrophages. EMBO J 2010;29:4223–4236
14. Clausen BE, Burkhardt C, Reith W, Renkawitz R, Förster I. Conditional gene targeting in macrophages and granulocytes using LysMcre mice. Transgenic Res 1999;8:265–277
15. Nakae J, Cao Y, Oki M, et al. Forkhead transcription factor FoxO1 in adipose tissue regulates energy storage and expenditure. Diabetes 2008;57:563–576
16. Fujisaka S, Usui I, Bukhari A, et al. Regulatory mechanisms for adipose tissue M1 and M2 macrophages in diet-induced obese mice. Diabetes 2009;58:2574–2582
17. Nakae J, Biggs WH 3rd, Kitamura T, et al. Regulation of insulin action and pancreatic beta-cell function by mutated alleles of the gene encoding forkhead transcription factor Foxo1. Nat Genet 2002;32:245–253
18. Furukawa S, Fujita T, Shimabukuro M, et al. Increased oxidative stress in obesity and its impact on metabolic syndrome. J Clin Invest 2004;114:1752–1761
19. Odegaard JI, Ricardo-Gonzalez RR, Goforth MH, et al. Macrophage-specific PPARgamma controls alternative activation and improves insulin resistance. Nature 2007;447:1116–1120
20. Mauer J, Chaurasia B, Plum L, et al. Myeloid cell-restricted insulin receptor deficiency protects against obesity-induced inflammation and systemic insulin resistance. PLoS Genet 2010;6:e1000938
21. Nakae J, Kitamura T, Silver DL, Accili D. The forkhead transcription factor Foxo1 (Fkhr) confers insulin sensitivity onto glucose-6-phosphatase expression. J Clin Invest 2001;108:1359–1367
22. Nakae J, Cao Y, Daitoku H, et al. The LXXLL motif of murine forkhead transcription factor FoxO1 mediates Sirt1-dependent transcriptional activity. J Clin Invest 2006;116:2473–2483
23. Kubota N, Kubota T, Itoh S, et al. Dynamic functional relay between insulin receptor substrate 1 and 2 in hepatic insulin signaling during fasting and feeding. Cell Metab 2008;8:49–64
24. Nakae J, Kitamura T, Kitamura Y, Biggs WH 3rd, Arden KC, Accili D. The forkhead transcription factor Foxo1 regulates adipocyte differentiation. Dev Cell 2003;4:119–129
25. Casamayor A, Morrice NA, Alessi DR. Phosphorylation of Ser-241 is essential for the activity of 3-phosphoinositide-dependent protein kinase-1: identification of five sites of phosphorylation in vivo. Biochem J 1999;342:287–292
26. Accili D, Arden KC. FoxOs at the crossroads of cellular metabolism, differentiation, and transformation. Cell 2004;117:421–426
27. Lehtinen MK, Yuan Z, Boag PR, et al. A conserved MST-FOXO signaling pathway mediates oxidative-stress responses and extends life span. Cell 2006;125:987–1001
28. Choi J, Oh S, Lee D, et al. Mst1-FoxO signaling protects naïve T lymphocytes from cellular oxidative stress in mice. PLoS ONE 2009;4:e8011
29. Yuan Z, Lehtinen MK, Merlo P, Villén J, Gygi S, Bonni A. Regulation of neuronal cell death by MST1-FOXO1 signaling. J Biol Chem 2009;284:11285–11292
30. Bi W, Xiao L, Jia Y, et al. c-Jun N-terminal kinase enhances MST1-mediated pro-apoptotic signaling through phosphorylation at Serine 82. J Biol Chem 2010;285:6259–6264
31. Nakae J, Barr V, Accili D. Differential regulation of gene expression by insulin and IGF-1 receptors correlates with phosphorylation of a single amino acid residue in the forkhead transcription factor FKHR. EMBO J 2000;19:989–996
32. Murano I, Barbatelli G, Parisani V, et al. Dead adipocytes, detected as crown-like structures, are prevalent in visceral fat depots of genetically obese mice. J Lipid Res 2008;49:1562–1568
33. Sauter NS, Schulthess FT, Galasso R, Castellani LW, Maedler K. The anti-inflammatory cytokine interleukin-1 receptor antagonist protects from high-fat diet-induced hyperglycemia. Endocrinology 2008;149:2208–2218
34. Naito M. Macrophage differentiation and function in health and disease. Pathol Int 2008;58:143–155
35. Hanisch UK, Kettenmann H. Microglia: active sensor and versatile effector cells in the normal and pathologic brain. Nat Neurosci 2007;10:1387–1394
36. Weisberg SP, McCann D, Desai M, Rosenbaum M, Leibel RL, Ferrante AW Jr. Obesity is associated with macrophage accumulation in adipose tissue. J Clin Invest 2003;112:1796–1808
37. Weisberg SP, Hunter D, Huber R, et al. CCR2 modulates inflammatory and metabolic effects of high-fat feeding. J Clin Invest 2006;116:115–124

Generation of induced pluripotent stem cells from primary chronic myelogenous leukemia patient samples

Keiki Kumano,[1,2] Shunya Arai,[1,2] Masataka Hosoi,[1,2] Kazuki Taoka,[1,2] Naoya Takayama,[3,4] Makoto Otsu,[5] Genta Nagae,[6] Koki Ueda,[1,2] Kumi Nakazaki,[1,2] Yasuhiko Kamikubo,[1,2] Koji Eto,[3,4] Hiroyuki Aburatani,[6] Hiromitsu Nakauchi,[3,5] and Mineo Kurokawa[1,2]

[1]Department of Hematology and Oncology, Graduate School of Medicine, University of Tokyo, Tokyo, Japan; [2]Core Research for Evolutional Science and Technology, Japan Science and Technology Agency, Tokyo, Japan; [3]Stem Cell Bank, Center for Stem Cell Biology and Regenerative Medicine, Institute of Medical Science, University of Tokyo, Tokyo, Japan; [4]Center for iPS Cell Research and Application, University of Kyoto, Kyoto, Japan; [5]Division of Stem Cell Therapy, Center for Stem Cell Biology and Regenerative Medicine, Institute of Medical Science, University of Tokyo, Tokyo, Japan; and [6]Genome Science Division, Research Center for Advanced Science and Technology, University of Tokyo, Tokyo, Japan

Induced pluripotent stem cells (iPSCs) can be generated by the expression of defined transcription factors not only from normal tissue, but also from malignant cells. Cancer-derived iPSCs are expected to provide a novel experimental opportunity to establish the disease model. We generated iPSCs from imatinib-sensitive chronic myelogenous leukemia (CML) patient samples. Remarkably, the CML-iPSCs were resistant to imatinib although they consistently expressed BCR-ABL oncoprotein. In CML-iPSCs, the phosphorylation of ERK1/2, AKT, and JNK, which are essential for the maintenance of both BCR-ABL (+) leukemia cells and iPSCs, were unchanged after imatinib treatment, whereas the phosphorylation of signal transducer and activator of transcription (STAT)5 and CRKL was significantly decreased. These results suggest that the signaling for iPSCs maintenance compensates for the inhibition of BCR-ABL. CML-iPSC–derived hematopoietic cells recovered the sensitivity to imatinib although $CD34^+38^-90^+45^+$ immature cells were resistant to imatinib, which recapitulated the pathophysiologic feature of the initial CML. CML-iPSCs provide us with a novel platform to investigate CML pathogenesis on the basis of patient-derived samples. (*Blood*. 2012;119(26):6234-6242)

Introduction

Hematologic malignancies including leukemias are often chemotherapy-resistant, most of which follows an aggressive clinical course.[1] Multiple drug therapies are usually required to treat them, although they are occasionally accompanied with many side effects. Thus, the invention of novel targeted therapies based on newly revealed molecular pathogenesis is expected to overcome the current situation.[2] However, previous approaches to understanding pathogenesis involve several limitations. Many mouse models of human diseases have been established, but they may not fully recapitulate many aspects of original human diseases.[3] Many kinds of cell lines are also available for research. However, they do not cover all diseases, because it is usually difficult to establish a cell line from a primary patient sample. Furthermore, additional gene mutations may be accumulated in cell lines. Theoretically, primary patient samples should be used for research, but the amount of obtained cells may be inadequate for various analyses.

Induced pluripotent stem cells (iPSCs) can be generated from various types of cells by the transduction of defined transcription factors.[4-10] In addition to the regenerative medicine,[11] iPSCs have been used for studies of the pathogenesis of inherited genetic diseases.[12-16] Recently, it was reported that iPSCs were generated not only from normal tissue cells, but also from malignant cells.[17-20] In those cases, cancer cells themselves must have been the origins of iPSCs. However, in most published data, established cell lines were used as the source material of cancer cells, including chronic myelogenous leukemia (CML),[17] gastrointestinal cancers,[18] and melanoma,[19] except for the JAK2-V617F mutation (+) polycythemia vera (PV) patient.[20]

CML is a myeloproliferative neoplasm that originates from hematopoietic stem cells transformed by the *BCR-ABL* fusion gene. The initial indolent chronic phase (CP) is followed by aggressive stages, the accelerated phase (AP), and the blast crisis (BC), in which immature leukemic cells expand.[21] CML is now initially treated with one of several tyrosine kinase inhibitors (TKIs) including imatinib, dasatinib, and nilotinib, which have dramatically improved the long-term survival rate of CML patients up to approximately 90%. However, even TKIs are not able to eradicate the CML clone completely, which is demonstrated by the fact that discontinuation of TKIs in molecular remission CML patients usually leads to the recurrence of the BCL-ABL clone. Therefore, many studies are performed to elucidate the mechanisms of TKI-resistance in CML stem cells and to overcome the resistance.

In this study, we established iPSCs from primary CML patient samples, redifferentiated them into hematopoietic lineage and showed the recapitulation of the pathophysiologic features of the initial disease.

Submitted July 14, 2011; accepted April 30, 2012. Prepublished online as *Blood* First Edition paper, May 16, 2012; DOI 10.1182/blood-2011-07-367441.

The online version of this article contains a data supplement.

The publication costs of this article were defrayed in part by page charge payment. Therefore, and solely to indicate this fact, this article is hereby marked "advertisement" in accordance with 18 USC section 1734.

Methods

Cell and cell culture

Primary samples of CML bone marrow cells were obtained after informed consent. All studies using human cells were reviewed and approved by the institutional review boards (IRBs) of University of Tokyo. Mononuclear cells (MNCs) were isolated by centrifugation through a Ficoll gradient. $CD34^+$ cells were isolated by an immunomagnetic separation technique (auto magnetic-activated cell sorting; MACS). They were cultured with α-minimum essential medium (MEM) containing 20% fetal calf serum (FCS) supplemented with 100 ng/mL stem cell factor (SCF; Wako), 10 ng/mL thrombopoietin (TPO; Wako), 100 ng/mL FL3L (Wako), 10 ng/mL IL3 (Wako), and 100 ng/mL IL6 (Wako).

Normal iPSCs established from cord blood (CB) $CD34^+$ cells or fibroblasts[22] and CML-iPSCs were maintained in Dulbecco modified Eagle medium-F12 (Invitrogen) supplemented with 20% knockout serum replacement (KSR; Invitrogen), 0.1mM 2-mercaptoethanol (Sigma-Aldrich), MEM nonessential amino acids (Invitrogen), and 5 ng/mL recombinant human basic fibroblast growth factor (FGF; Peprotech) on mitomycin C (MMC)–treated mouse embryo fibroblast (MEF) feeder cells.[23] Imatinib (LC Laboratories) was added to the culture medium at the various concentrations (1-10μM). U0126 and LY294004 (LC Laboratories) were used to inhibit ERK and AKT, respectively.

The mouse C3H10T1/2 cells were cultured as previously described.[24]

Production of VSV-G pseudotyped retroviral particles

Construction of pMXs vectors encoding Oct3/4, Sox2, Klf4, and c-myc were performed as previously described.[22] Highly concentrated VSV-G–pseudotyped retroviral supernatant was prepared using reported procedures. The 293GPG cells were kind gifts from Dr R. C. Mulligan (Children's Hospital Boston, Harvard Medical School, Boston, MA).[25] Stable 293GPG cell lines, each capable of producing VSV-G–pseudotyped retroviral particles on induction were established as previously described.[22,25] Retroviral supernatants were concentrated by centrifugation for 16 hours at 6000*g*.

Generation of iPSCs from CML samples

Two days before infection, cells were stimulated with cytokines as mentioned in "Cell and cell culture." For infection, each well of a 24-well dish coated with a fibronectin fragment CH296:RetroNectin (Takara-Bio) was covered with virus-containing supernatants. After the adhesion of viruses according to the manufacture's recommendation, 1×10^5 cells of $CD34^+$ CML cells or CB cells were inoculated into each well and filled with the culture medium supplemented with cytokines. The next day, concentrated viral supernatant was added to the culture. On day 3 after infection, cells were harvested with vigorous pipetting, washed by phosphate-buffered saline (PBS), and cultured with the same fresh medium for next 3 days. On day 6, cells were seeded on MMC treated MEF cells. Two to 4 days after, the medium was replaced with human ES medium as previously described with 0.5mM valproic acid (VPA; Sigma-Aldrich).[26] Subsequently, medium was changed every other day. After 20 days, ES-like colonies appeared. Using live cell imaging technology with Tra-1-60 antibody as previously described,[27] each fully reprogrammed colony was distinguished from deficiently reprogrammed colonies, and was picked up to be reseeded on new MEF feeder cells. Cloned ES-like colonies were subjected to further analysis.

Antibodies, FACS analysis, and immunocytochemistry

The following fluorescent conjugated antibodies were used for fluorescence-activated cell sorter (FACS) analysis and immunocytochemistry: anti–human stage specific embryonic antigen (SSEA)–4 conjugated with Alexa Fluor 488 (BD Bioscience), anti–human tumor related antigen (TRA)–1-60 conjugated with Alexa Fluor 555 (BD Bioscience), anti-CD34 phycoerythrin (PE) conjugated (Beckman Coulter), and anti-CD45 fluorescein isothiocyanate (FITC) conjugated (Beckman Coulter).

Cells were sorted with a FACSAria, and analysis was performed on FACS LSRII (BD Bioscience).

For immunocytochemistry, cells were fixed with 4% paraformaldehyde in PBS, after which they were labeled with an antibody against human SSEA-4 and antibody against human TRA-1-60 antibody and observed using a confocal microscope (Carl Zeiss).

Methylation profiling

Genomic DNA was extracted using the QIAamp DNA Mini Kit (QIAGEN) according to the manufacture's instruction. Methylation status was evaluated as previously reported.[28] Methylation status was analyzed using HumanMethylation27 BeadChip (Illumina). Genomic DNA for methylation profiling was quantified using the Quant-iT dsDNA BR assay kit (Invitrogen). Five-hundred nanograms of genomic DNA was bisulfite-converted using an EZ DNA methylation kit (Zymo Research). The converted DNA was amplified, fragmented and hybridized to a beadchip according to the manufacturer's instructions. The raw signal intensity for both methylated (M) and unmethylated (U) DNA was measured using a BeadArray Scanner (Illumina). The methylation level of the each individual CpG is obtained using the formula (M)/(M) + (U) + 100 by the GenomeStudio (Illumina).

Microarray analysis

Gene expression analysis was carried out as previously described[29] with the use of the Human Genome U133 Plus 2.0 Array (Affymetrix). The hierarchical clustering techniques classify data by similarity and their results are represented by dendrograms. Previously reported data of human embryonic stem (ES) cells (GSM449729) and CML $CD34^+$ cells (GSM366215, 366216, 366221, and 366222) were used to compare the gene expression profile. The microarray data are available on the Gene Expression Omnibus (GEO) database under accession number GSE37982.

Hematopoietic differentiation of iPSCs

To differentiate iPSCs into hematopoietic cells, we used the same protocol previously used with ES cells and iPSCs.[22,24] In brief, small clusters of iPSCs (< 100 cells treated with PBS containing 0.25% trypsin, 1mM $CaCl_2$, and 20% KSR) were transferred onto irradiated 10T1/2 cells and cocultured in hematopoietic cell differentiation medium, which was refreshed every third day. Differentiation medium consists of Iscove modified Dulbecco medium supplemented with a cocktail of 10 μg/mL human insulin, 5.5 μg/mL human transferrin, 5 ng/mL sodium selenite, 2mM L-glutamine, 0.45mM α-monothioglycerol, 50 μg/mL ascorbic acid, and 15% highly filtered FBS in the presence of 20 ng/mL human vascular endothelial growth factor (VEGF).[24] On days 14 to 15 of culture, the iPS-sacs were collected into a 50-mL tube, gently crushed with a pipette tip and passed through a 40-μm cell strainer to obtain hematopoietic progenitors. Hematopoietic progenitors were collected by sorting with CD34 and CD45 antibodies, Giemsa stained, and then examied under a microscope. Hematopoietic progenitors were cultured in the α-medium plus 20% FCS supplemented with 100 ng/mL SCF, 10 ng/mL TPO, 100 ng/mL FL3L, 10 ng/mL IL3, and 100 ng/mL IL6.

Hematopoietic colony-forming cell (CFC) assay

CFC assays were performed in MethoCult H4434 semisolid medium (StemCell Technologies). Ten thousand hematopoietic progenitors harvested from an iPS-Sacs were plated in 1.5 mL of medium and cultivated for 14 days.

RT-PCR and quantitative real-time PCR analysis

After extraction of total RNA with RNAeasy reagents (QIAGEN), reverse transcription was performed with SuperScript III (Invitrogen). Primer

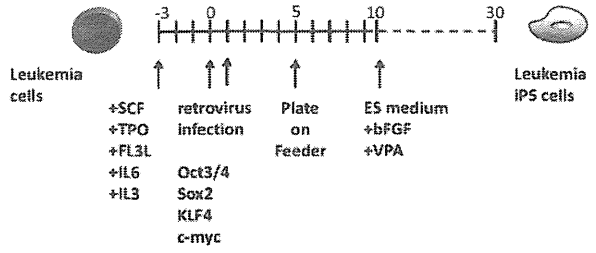

Figure 1. Experimental scheme for generating of iPSCs from the CML patient sample. After cytokine stimulation, $CD34^+$ CML cells were reprogrammed by transduction with Yamanaka factors. To improve the reprogramming, valproic acid was added to the culture.

sequences used for the detection of stem cell genes were as previously described.[9]

Quantitative real-time PCRs (qPCRs) were carried out in the ABI-7000 sequence detection system with SYBR Green PCR Core reagents according to the manufacturer's instructions (Applied Biosystems). We analyzed expression levels of *BCR-ABL* fusion transcript as previously described.[30] Each assay was performed in triplicate and the results were normalized to GAPDH (glyceraldehyde-3-phosphate dehydrogenase) levels.

PCR primers used for quantitative PCR:

BCR-ABL F TCAGAAGCTTCTCCCTGACATCCGT

BCR-ABL R TCCACTGGCCACAAAATCATACAGT

GAPDH F TGCACCACCAACTGCTTAGC

GAPDH R GGCATGGACTGTGGTCATGAG

Western blotting

Fifty micrograms of cell lysates were subjected to sodium dodecylsulfate-polyacrylamide gel electrophoresis (SDS-PAGE) and Western blot analysis. Antibodies used in immunoblotting were as follows; anti-phospho ERK1/2 (Thr202/Tyr204; Cell Signaling), anti-phospho Akt (Ser473; Cell Signaling), anti-phospho JNK (Thr183/Tyr185; Cell Signaling), anti-phospho-STAT5 (Tyr694; Cell Signaling), and anti-phospho CRKL (Tyr207; Cell Signaling). Enhanced chemiluminescence detection (Amersham) was carried out according to the manufacturer's recommendations.

Results

Generation of iPSCs from primary CML patient samples

After obtaining informed consent, $CD34^+$ cells were purified from bone marrow mononuclear cells of a CML chronic phase patient. After we stimulated them with cytokines for 2 days, retroviral transduction with the transcription factors OCT3/4, SOX2, KLF4, and MYC was performed. Two days after transduction, we reseeded cells onto MEF cells and cultured them for another 2 days. Then, we replaced the medium with human ES medium supplemented with 5 ng/mL bFGF. To improve the efficiency of the reprogramming, we added VPA,[26] a histone deacetylase inhibitor, to the culture (Figure 1). Using a live cell imaging method with Tra-1-60 antibody, bona fide iPSCs were distinguished from deficiently reprogrammed cells.[27] As a result, 2 CML-derived iPSCs (CML-iPSCs) were generated, which were derived from independent patients. CML-iPSCs showed the typical morphology as iPSCs (Figure 2A) and expressed the pluripotency markers, such as SSEA-4 and Tra-1-60 (Figure 2B), and the endogenous expression of embryonic stem cell (ESC) characteristic transcripts (OCT3/4, SOX2, KLF4, NANOG, LIN28, and REX1) was confirmed by RT-PCR (Figure 2C). CML-iPSCs also expressed BCR-ABL, which demonstrated that they were truly derived from CML (Figure 2D). Furthermore, fluorescence in situ hybridization with dual color *BCR-ABL* probes confirmed t(9;22) translocation in CML-iPSCs at the single cell level (supplemental Figure 1A and supplemental Table 1, available on the *Blood* Web site; see the Supplemental Materials link at the top of the online article). However, although CML-iPSCs expressed BCR-ABL, they were resistant to imatinib (Figure 2E). Teratoma formation capacity was confirmed, demonstrating the pluripotency of CML-iPSCs (supplemental Figure 2).

Comprehensive analysis of DNA methylation revealed that methylation pattern of CML-iPSCs was different from that of original CML sample but was very similar to that of normal iPSCs although there were slight differences (Figure 3A). Previously, stem cell–specific differentially methylated regions (SS DMRs)

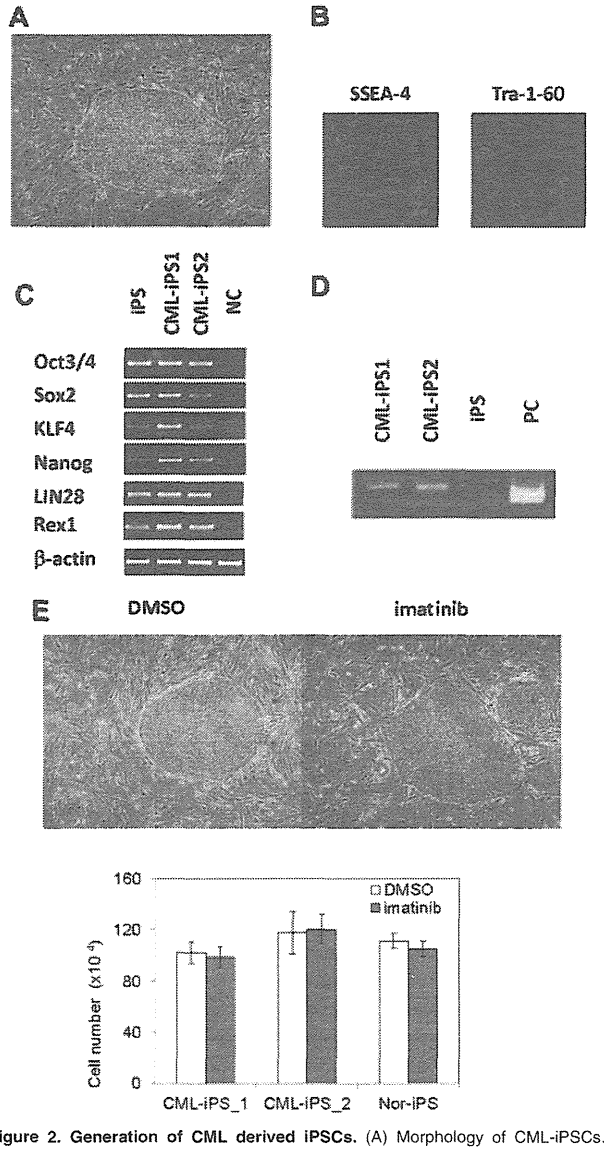

Figure 2. Generation of CML derived iPSCs. (A) Morphology of CML-iPSCs. (B) Immunofluirescence staining shows expression of pluripotent marker (left: SSEA-4 and right: Tra-1-60) in CML-iPSCs. (C) RT-PCR analysis of ES cell marker genes. Endogenous expression of these stem cell–specific genes in CML-iPSCs was verified. (D) CML-iPSCs expressed the BCR-ABL fusion transcript. (E) Imatinib (10μM) were added to the culture of iPSCs. DMSO (top left panel) and imatinib (top right panel) treated CML-iPSCs were shown. The number of alive CML-iPSCs (CML-iPS_1 and CML-iPS_2) and normal iPSCs (Nor-iPS) after 5 days treatment was calculated (bottom panel). These were the representative data from 3 independent experiments.

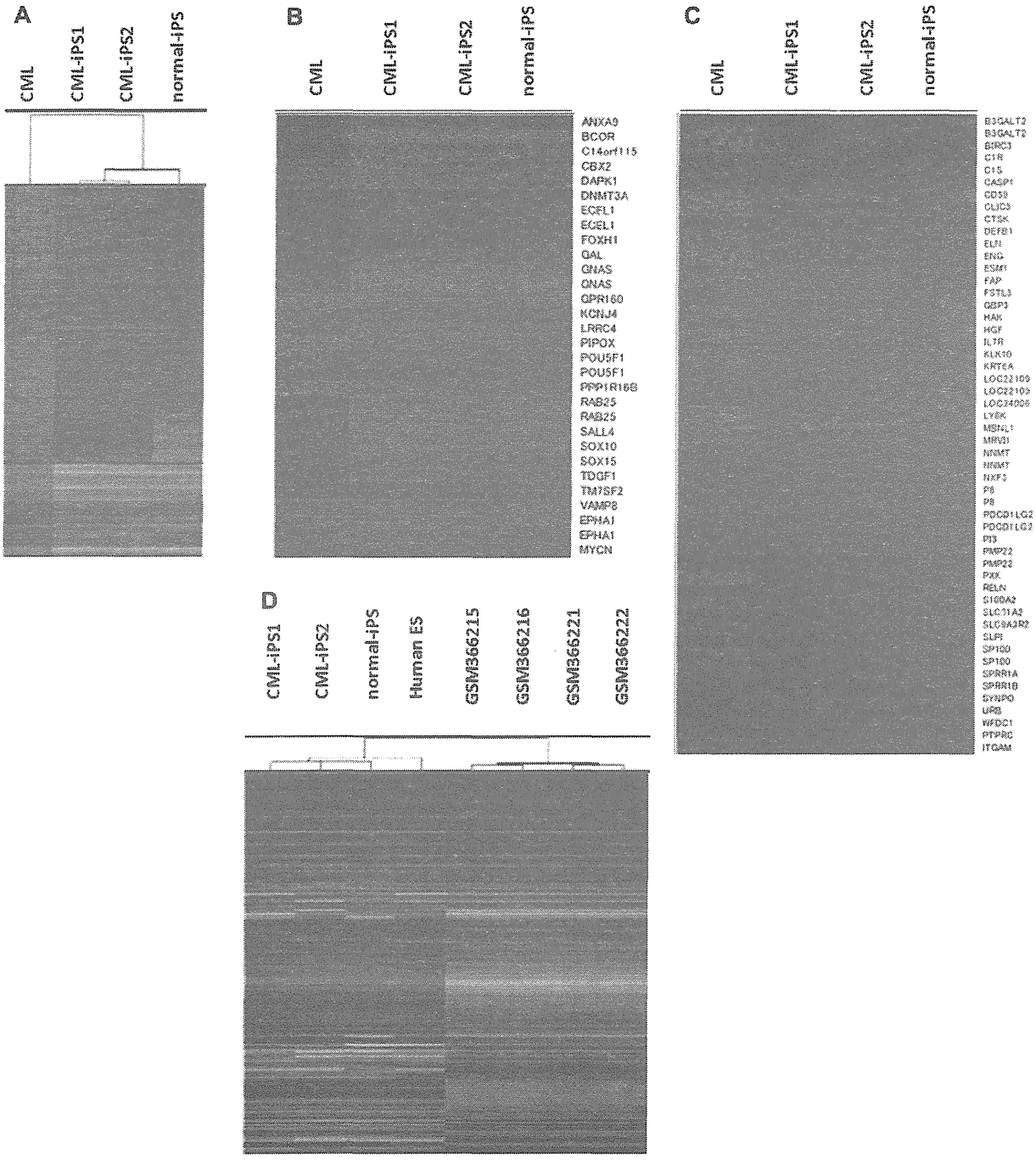

Figure 3. Comprehensive analysis of DNA methylation and gene expression. (A) Unsupervised hierarchical clustering based on differentially methylated CpGs is shown on the dendrogram. The accompanying heatmap shows the methylation status across 5001 differentially methylated CpGs. In the heatmap, red indicates a CpG methylation more than 50%, and green less than 50%. The methylation status in hypo SS DMRs (B) or hyper SS DMRs (C) was shown in the heatmap. (D) Unsupervised hierarchical clustering based on global gene expression data are shown on the dendrogram. The accompanying heatmap shows the normalized log2 transformed expression values (Z-scores) for each probe. In the heatmap, red indicates expression more than mean, and green less than mean.

were identified during reprogramming process of iPSCs.[31] Hypomethylated SS DMRs (hypo SS DMRs) in the variety of iPSCs were also hypomethylated in the CML-iPSCs including the promoters of OCT4 (Figure 3B). In the same way, hypermethylated SS DMRs (hyper SS DMRs) in the variety of iPSCs were also hypermethylated in the CML-iPSCs (Figure 3C). The promoters of hematopoietic lineage-specific marker genes, such as CD45 and CD11b, were hypermethylated in the CML-iPSCs. Thus, the methylation pattern of CML-iPSCs was confirmed to be not hematopoietic cell-like, but iPSC-like. Next, we compared the gene expression pattern among CML-iPSCs and normal iPSCs (Figure 3D). In a result, CML-iPSCs and normal iPSCs were very similar in regard to global gene expression profile. Furthermore, comparing our results with publicly available expression data of human ES cells and CML $CD34^+$ cells, we found that CML-iPSCs were very similar to human ES cells, whereas they were different

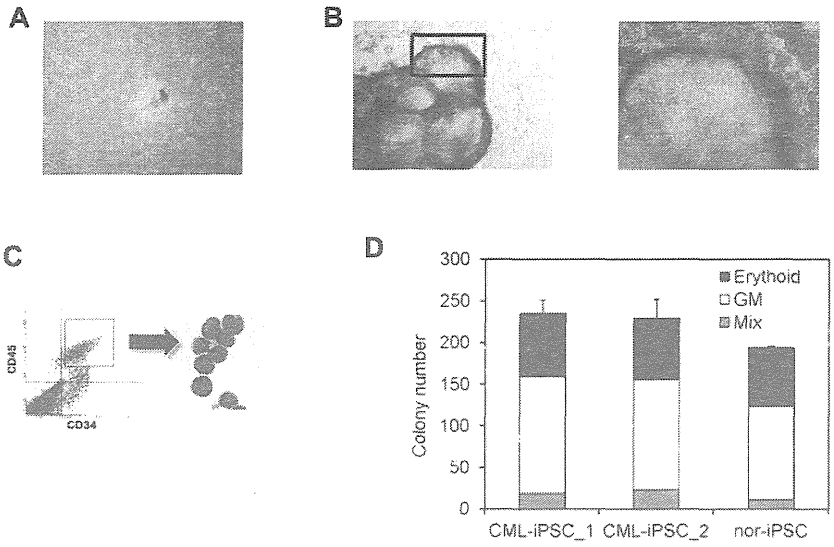

Figure 4. Hematopoietic differentiation of CML-iPSCs. CML-iPSCs were differentiated on the 10T1/2 cells. On day 7 (A), iPSCs began to mount. On day 14 of culture (B: left panel), inflated sac-like structures appeared. These sac-like structures contained the round hematopoietic cells (B: right panel: higher magnification). (C) These hematopoietic cells expressed immature marker CD34 and CD45. (D) CFC activity was estimated using 1×10^4 3CD34$^-$ CD45$^+$cells. Erythroid colonies (black bars), granulocyte-monocyte (GM) colonies (white bars), and mixed GM colonies with erythtoid cells (mix: gray bars) were plotted.

from CML CD34$^+$ cells in terms of gene expression patterns (Figure 3D).

Hematopoietic differentiation of CML-iPSCs

Then we differentiated them into hematopoietic progenitors within the "unique sac-like structures" (iPS-sacs: Figure 4A-B). This method was reported to be able to produce the hematopoietic progenitors with higher efficiency than the usual embryoid body formation method using human ESCs and iPSCs.[22,24] On day 15 of culture, iPSCs sacs contained round hematopoietic-like cells (Figure 4B). Then we picked up iPS-sacs with a pipette tip and dissociated them mechanically and obtained the inner round cells. Round cells, positive for a hematopoietic lineage marker CD45 and an immature marker CD34, proved to be hematopoietic progenitors (Figure 4C).

Then we characterized the CML-iPSCs derived hematopoietic cells, comparing with those derived from normal iPSCs. CFC activities were measured using the same number of CD34$^+$ cells (Figure 4D). Hematopoietic progenitors derived from CML-iPSCs and normal iPSCs produced colonies of mature erythroid, granulocyte-macrophage, or mixed of these hematopoietic cells in growth factor-supplemented methyl cellulose medium with a similar distribution of colony size, morphologies, and kinetics of growth and maturation. The colony forming cells expressed BCR-ABL (supplemental Figure 1B and supplemental Table 2).

Next, we tested the engraftment potential of these cells. nonobese diabetic/severe combined immunodeficiency IL2Rg deficient (NOG) mice serve as a superior host for engraftment of human normal and malignant hematopoietic cells.[32] One million CD34$^+$ cells were intravenously transplanted into NOG mice with minimal irradiation (2 Gy; supplemental Figure 3A). Only transient engraftment was observed and the recipient mice never showed CML phenotype in vivo (supplemental Figure 3B).

BCR-ABL dependence is lost in the CML-iPSCs

The restricted dependence of BCR-ABL signaling on survival of CML cells enables the disease suppression by imatinib and dramatically changed the CML treatment after the development of imatinib.[33] CML patients whose cells were used for the generation of iPSCs effectively responded to imatinib therapy. However, although CML-iPSCs expressed BCR-ABL, they were resistant to imatinib (Figure 2E). Interestingly, CML-iPSC–derived hematopoietic cells recovered the sensitivity to imatinib except CD34$^+$38$^-$90$^+$45$^+$ immature cell population, which recapitulated the feature of initial CML disease (Figure 5A). Various concentrations of imatinib were added to the culture of iPSC derived hematopoietic cells. Similar kinetics of imatinib response between CML-iPSC–derived hematopoietic cells and imatinib sensitive CML cell line K562 was observed (Figure 5B). Furthermore, we generated CD34$^+$CD38$^-$CD90$^+$CD45$^+$ cells from CML-iPSCs. Surprisingly, this fraction of phenotypically immature cells showed the imatinib resistance like CML-iPSCs although more differentiated cells (CD34$^-$CD45$^+$) showed the sensitivity to imatinib (Figure 5C).

Then, we investigated why CML-iPSCs showed the imatinib-resistance. It was reported that imatinib resistant patients sometimes express higher BCR-ABL transcript than imatinib sensitive patients.[34] In addition, CML leukemia stem cells showed higher BCR-ABL expression than differentiated CML cells.[35] Therefore, we examined the BCR-ABL mRNA expression levels in the CML-iPSCs, and compared them with the primary CML sample, and CML-iPSC–derived hematopoietic cells. As a result, BCR-ABL expression was not increased in CML-iPSCs compared with the primary CML sample and CML-iPSCs–derived hematopoietic cells. (Figure 6A)

BCR-ABL activates Ras-MAPK, PI3K-AKT, JAK-STAT pathways. Among them, it was reported that STAT5, ERK1/2, JNK, and AKT are essential for the survival of BCR-ABL–dependent leukemic cells.[36,37] In addition, CRKL is another direct target of BCR-ABL.[38] The phosphorylation status of ERK1/2, AKT, JNK, and STAT5 in CML-iPSCs, which are essential for the survival of BCR-ABL (+) hematopoietic progenitors, were evaluated after imatinib treatment. The phosphorylation of ERK1/2, AKT, and JNK, which are also essential for the maintenance of iPSCs and ES cells,[39,40] were unchanged after treatment in the CML-iPSCs although they were decreased in the CML-iPSCs–derived hematopoietic cells (Figure 6B). The phosphorylation of CRKL and STAT5, which were not activated in the normal iPSCs, was decreased in both CML-iPSCs and CML-iPSCs–derived hematopoietic cells (Figure 6B). These results showed that the signaling for iPSCs maintenance

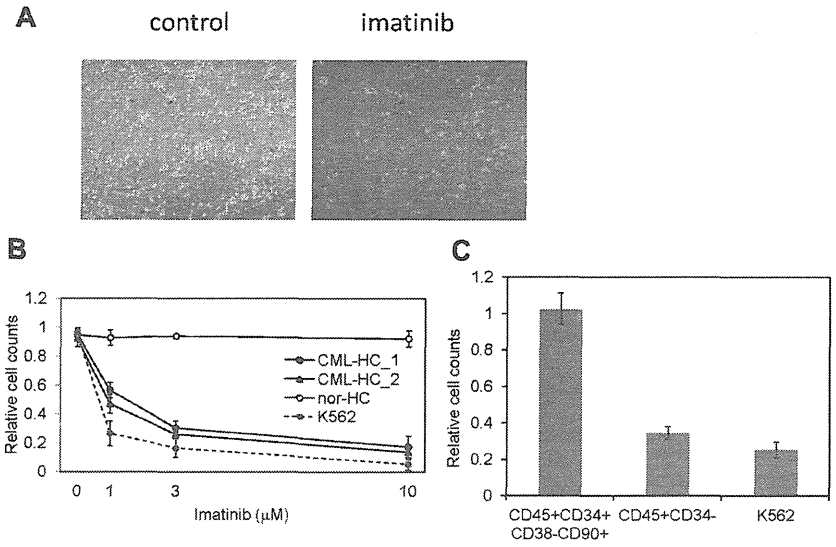

Figure 5. CML-iPSC derived hematopoietic cells recovered the sensitivity to imatinib. (A) Imatinib but not the vehicle (DMSO) decreased the growth of hematopoietic cells derived from CML-iPSCs in suspension culture. (B) Various concentrations of imatinib were added to the culture of iPSC derived hematopoietic cells for 4 days. CML-iPSC–derived $CD34^-$ hematopoietic cells (CML-HC_1 and CML-HC_2), normal iPSC-derived hematopoietic cells (nor-HC), and K562 cells were used for analyses. *Relative cell counts compared with the vehicle* control were plotted. Shown is the mean of a single experiment conducted in triplicate as a representative of 3 independent experiments. (C) Imatinib (10μM) was added to the suspension culture of CML-iPSC–derived hematopoietic cells for 4 days. The immature cell fraction ($CD34^+CD38^-CD90^+CD45^+$) showed resistance similar to CML-iPSCs, although more differentiated cells ($CD34^-CD45^+$) showed the sensitivity to imatinib. Relative cell counts compared with the vehicle control was plotted.

might compensate for the inhibition of BCR-ABL in CML-iPSCs and that BCR-ABL dependence was lost in CML-iPSCs. In addition, the specific inhibitor of ERK or AKT signaling worked as expected, respectively (Figure 6C), resulting in the reduction of attached cells regardless of the addition of imatinib (Figure 6D).

Discussion

Generation of CML-derived iPSCs

We generated iPSCs from primary CML patient samples. Methylation pattern and gene expression of CML-iPSCs were very similar to those of normal iPSCs. Previously, SS DMRs were identified during reprogramming process of iPSCs.[31] Hypo SS DMRs were also hypomethylated in the CML-iPSCs (Figure 3B). Among them, some genomic regions, such as the promoter of N-MYC, had already been hypomethylated in the primary CML sample. In the same way, some genes associated with hyper SS DMRs had already been hypermethylated in the primary CML sample (Figure 3C). However, we could not detect the CML-iPSC–specific DMRs in this study. Then, we redifferentiated them into hematopoietic lineage and showed the recapitulation of the features of the initial disease. In addition, although CML-iPSCs expressed BCR-ABL, it was surprising that there were no obvious differences of gene expression profile between normal iPSCs and CML-iPSCs (Figure 3D). The results that inhibition of BCR-ABL by imatinib did not affect CML-iPSC survival indicate that signaling of BCR-ABL might not be important in iPSCs. These results are consistent with the gene expression profile data in which the effect of BCR-ABL signaling was hardly observed. One possibility is that global tyrosine kinase activities and downstream signaling pathways would be so activated in iPSCs irrespective of BCR-ABL that BCR-ABL no longer adds significant effects.

CML is known to be a clonal disorder originated from hematopoietic stem cells caused by BCR-ABL fusion gene. Although BCR-ABL TKI imatinib can reduce CML cells below the detection of molecular level, its discontinuation often results in the rapid relapse of leukemia.[41] These results indicate the existence of CML stem cells, which are resistant to the TKI. CML stem cells are thought to be included in the primitive population ($CD34^+CD38^-$). According to some published data, they have lost the addiction to BCR-ABL[42,43] In addition, CML-iPSCs also have shown resistance to the imatinib.[44] Furthermore, in our experiments, immature $CD34^+38^-90^-45^+$ cells differentiated from CML-iPSCs also showed imatinib resistance similar to CML-iPSCs, although more differentiated cells ($CD34^-CD45^+$) showed sensitivity to imatinib (Figure 5C). So, these immature cells showed a phenotype of CML stem cells. Imatinib treatment of CML stem cells decreased the phosphorylation of CRKL and STAT5 but not of AKT,[42] as shown in the CML-iPSCs described here. There may be some shared mechanism between CML stem cells and CML-iPSCs. For example, Wnt-β-catenin signaling is essential for the maintenance of both CML stem cells and iPSCs.[45,46] Using immature cells obtained in our study, the mechanism of imatinib resistance of CML stem cells can be further investigated.

Previously, it was reported that primary CML samples and the CML BC cell line KBM7 were reprogrammed and that primary CML-iPSCs[47] and KBM7-iPSCs were established.[17] As shown here, KBM7-iPSCs lost the BCR-ABL dependence and became resistant to imatinib, although primary CML-derived iPSCs were not checked for the imatinib sensitivity. Carette et al argued that a specific differentiated epigenetic cell state is needed to maintain BCR-ABL dependence.[17] However, they only showed the BCR-ABL expression but did not confirm BCR-ABL activation in the KBM7-iPSCs. We showed BCR-ABL specific phosphorylation of STAT5 and CRKL although they were not necessary for the survival of iPSCs and that imatinib treatment inhibits these signaling. On the other hand, RAS-MAPK and PI3K-AKT signaling were unchanged after imatinib treatment. It was reported that inhibition of caspase-mediated anoikis by bFGF is dependent on activation of ERK and AKT in human ES cells.[39] We also showed that the inhibition of ERK or AKT irrespective of the presence of the imatinib resulted in the decrease of the attached cell numbers. Some key molecules essential for the maintenance of iPSCs may compensate for the BCR-ABL inhibition in the CML-iPSCs through downstream ERK and AKT signaling pathways. They may include contact-mediated signaling with stem cell niches, and may be shared with CML stem cells and CML-iPSCs.